NANOSTRUCTURED IMMUNOSENSOR FOR LOW LEVEL DETECTION OF WATERBORNE *CRYPTOSPORIDIUM*

UNIVERSITY *of the*
WESTERN CAPE

Andrea Martha Siwak

A mini thesis submitted in partial fulfilment of the requirements for the degree of

Magister Scientiae in Nanoscience

Department of Medical Bioscience

University of the Western Cape

03 December 2022

Supervisor: Prof Admire Dube

Co-supervisor: Prof Priscilla Baker

KEYWORDS

Cryptosporidium

Oocysts

Cryptosporidiosis

Waterborne disease

Detection

Nanoscience

Nanotechnology

Gold nanoparticles

Synthesis

Characterization

Spectroscopy

Microscopy

Biosensor

Immunosensor

Cyclic voltammetry

Electrochemistry

ABSTRACT

A major causative agent of gastrointestinal disease is *Cryptosporidium*, a protozoan waterborne parasite identified in over 70 countries. *Cryptosporidium* infection is a cause of high disease morbidity in children and the immunocompromised, with limited treatment options available for patients at risk of severe illness. The hardy nature of the organism leads to the persistence of its oocyst form in drinking water sources, with standard water treatment procedures such as chlorine disinfection and activated sludge proving inefficient for its removal from effluent water. Studies indicate that *Cryptosporidium* is emerging as a major human pathogen in the developing world, and prevalence rates in South African communities have been found to range between 5.7-67.8%.

Detection of oocysts in water sources for disease prevention is suboptimal due to large required sample volumes, lengthy processing times, low sensitivity and high cost of equipment and reagents for analysis. A need for improvement exists to identify the organism as an emerging threat in domestic water systems, and the technological advantages that nanoparticle-based biosensors promise over current analytical methods, such as increased sensitivity, may offer a feasible preventative approach to outbreaks of *Cryptosporidium*. While current protocols for detection of *Cryptosporidium* vary, the gold standard is the EPA-1623.1 method which can be divided into four steps: 1) filtration or continuous flow centrifugation of at least 10L of water for preconcentration 2) separation of oocysts from background by immunomagnetic separation (IMS) 3) staining with fluorescently labelled antibodies and 4) fluorescence microscopy.

The aim of this project was the fabrication of a highly sensitive electrochemical immunosensor for *Cryptosporidium* detection in water samples. The immunosensor was composed of a gold nanoparticle-modified glassy carbon electrode functionalized with anti-*Cryptosporidium* mouse monoclonal IgG3 antibody. The target of the antibody was a membrane antigen of *Cryptosporidium* to facilitate the selective capture of oocysts at the electrode surface. The immunosensor was hence designed as a label-free system whereby detection of bound oocysts was achieved

electrochemically by capturing the change in signal with cyclic voltammetry when oocysts bound to the glassy carbon/gold nanoparticle interface. As oocysts do not have an inherent electrochemical signal, the redox mediator ferricyanide was used to provide a measurable electrochemical signal, where the decrease in peak current was used as a measure of oocyst binding to the electrode surface.

Gold nanoparticles were synthesized using the Turkevich method and characterized using ultraviolet-visible spectroscopy, dynamic light scattering, transmission electron microscopy and atomic force microscopy. The immunosensor was fabricated by drop casting the gold nanoparticles on the surface of a glassy carbon electrode, and physical immobilization of the anti-*Cryptosporidium* mAb onto the gold nanoparticles. The electrochemical behaviour of the immunosensor was characterized by cyclic voltammetry scan rate studies, where the gold nanoparticles were confirmed to enhance the electron migration of the system and increase the diffusion coefficient from 2.60 $m^2.s^{-1}$ of the bare electrode to 2.73 $m^2.s^{-1}$ in the gold modified electrode. The sensitivity of the immunosensor was shown to be high, with a limit of detection of 7.32 and 6.09 oocysts.mL^{-1} for the oxidation and reduction processes, respectively, and a limit of quantification of 22.19 and 18.47 oocysts.mL^{-1}.

DECLARATION

I declare that *Nanostructured immunosensor for low level detection of waterborne Cryptosporidium* is my own work, that it has not been submitted for any degree or examination in any other university, and that all the sources I have used or quoted have been indicated and acknowledged by complete references.

Full name...Andrea Martha Siwak..... Date.....03/12/2022.....

Signed..... 

ACKNOWLEDGEMENTS

I would like to express my gratitude and appreciation to:

Prof Admire Dube and Prof Priscilla Baker who supported my research interests, guided my progress and aided with the preparation of this mini thesis.

My husband Louis who raised my spirits in tough times, encouraged me when I was uninspired, and supported me throughout my entire academic career.

My parents and siblings for always encouraging me to continue my studies and supporting me in all of my endeavours.

Ms Valencia Jamalie and Prof Lindsay for their unending assistance and accommodation.

The MSc Nanoscience class of 2021-2022.

The late Mr Hoare, my high school science teacher who sparked and cultivated my interest with his love for the field.

The Department of Science and Innovation for funding my studies.

Contents

LIST OF ABBREVIATIONS

AIDS – Acquired immunodeficiency syndrome

AFM – Atomic force microscopy

ART – Antiretroviral therapy

AuNP – Gold nanoparticles

CD4 – Cluster of differentiation 4

DFA – Direct immunofluorescence assay

DAPI - 4′,6-diamidino-2-phenylindole

DIC – Differential interference contrast

DNA – Deoxyribonucleic acid

DLS – Dynamic light scattering

EDC - 1-Ethyl-3-(3-dimethylaminopropyl)carbodiimide

EDS – Energy-dispersive x-ray spectroscopy

ELISA – Enzyme-linked immunosorbent assay

FDA – Food and drug administration

FITC - Fluorescein isothiocyanate

HIV – Human Immunodeficiency Virus

IgG - Immunoglobulin G

IgM – Immunoglobulin M

IMS – Immunomagnetic separation

ITO – Indium tin oxide

LOD – Limit of detection

LOQ – Limit of quantification

mAb – Monoclonal antibody

mL – millilitre

mRNA – Messenger ribonucleic acid

NHS – N-hydroxy-succinimide

PBS – phosphate-buffered saline

PEMC - Piezoelectric-excited millimetre-sized cantilevers

SANS – South African National Standard

SELEX – Systemic evolution of ligands by exponential enrichment

SEM – Scanning electron microscopy

SERS – Surface-enhanced Raman spectroscopy

SERRS – Surface-enhanced resonance Raman spectroscopy

SPR – Surface plasmon resonance

US EPA – United States Environmental Protection Act

UV-Vis – Ultraviolet-visible spectroscopy

LIST OF FIGURES

LIST OF TABLES

1. Chapter 1: Introduction

This chapter introduces the background of the parasite *Cryptosporidium* and focuses on the health impact this parasite causes, both globally and locally in South Africa, particularly for the immunosuppressed. The problem statement and aims and objectives of this study are also presented.

1.1 Introduction

The Apicomplexan protozoan parasite *Cryptosporidium* is the etiological agent of the potentially life-threatening waterborne gastrointestinal disease cryptosporidiosis, first identified in humans in 1976 [1]. *Cryptosporidium* can infect a wide variety of vertebrate animals, and genotype names are designated after the host specificity of the strain. Infection in humans is most commonly caused by *C. hominis* or the cattle genotype *C. parvum*, although other species such as *C. meleagridis, C. felis,* and *C. canis* occasionally cause human infection [2]. The intricate life cycle of *Cryptosporidium* is characteristic of members of the phylum *Apicomplexa*. The parasite completes its life cycle in a single host undergoing both asexual and sexual reproductive cycles. Infection begins with the ingestion of highly infectious *Cryptosporidium* oocysts, which multiply in the small intestine and are excreted in large numbers to contaminate the environment and replicate the cycle in another host.

Cryptosporidiosis is a major cause of childhood mortality globally, but particularly in low-resource settings, and burden of disease is high among the immunosuppressed and immunodeficient. In immunocompetent hosts diarrhoea is acute and self-limiting, generally resolving in less than two weeks [3]. Conversely, infection is persistent and recurring in immunocompromised hosts and can lead to life-threatening malabsorption and dehydration, resulting in significant morbidity and mortality. The global burden of cryptosporidiosis is believed to be highly underestimated as diagnostic tests are underused and have poor sensitivity [4], and treatment options are limited for patients at high risk of serious illness.

Despite being identified as one of four key pathogens that cause the majority of moderate to severe childhood diarrhoeal cases [5], *Cryptosporidium* is the only one without an effective vaccine or treatment. This lag in pharmaceutical development is due in part to the lack of accessible animal infection models and in vitro culture methods that can reproduce the entire *Cryptosporidium* life cycle [6]. Hence, public health approaches such as thorough sanitation measures, filtration, disinfection and testing of drinking water supplies are crucial for disease prevention in the absence of efficacious therapeutics.

1.2 Organism Overview and Life Cycle

The *Cryptosporidium* life cycle begins with the ingestion of fully sporulated, thick-walled oocysts by the host. The oocysts are 4-6 µm in diameter and contain four naked sporozoites [2]. *Cryptosporidium* oocysts are highly infectious, with human volunteer studies showing that as few as 1-10 *C. hominis* oocysts can cause disease in healthy adults [7]. Additionally, oocysts are resistant to prolonged environmental exposure and common disinfection agents [8], due to *Cryptosporidium* oocyst wall proteins (COWPs) forming extensive disulphide bridges and providing high mechanical strength to the oocyst wall. Activation of the oocysts is triggered by the temperature and pH conditions of the gastrointestinal tract, causing oocysts to excyst in the upper small intestine and release the spindle-shaped sporozoites as shown in Figure 1.1 [3]. The sporozoites penetrate the mucous layer of the intestines, attaching to nearby enterocytes via the apical complex and causing the engulfment of the parasite which forms a parasitophorous vacuole.

The vacuole is located within the host cell plasma membrane but is separated from the host cytoplasm by a feeder organelle and cytoskeletal elements, forming a pathway for sporozoite access to nutrients to allow for differentiation into the trophozoite form [3]. Trophozoites undergo mitotic division to form meronts, and merozoites bud off from the meronts to escape the vacuole and be engulfed as previously described by adjacent enterocytes. The purpose of this process is to increase parasitic numbers in the host, however, some merozoites instead differentiate into the sexual macro and microgamont forms [9].

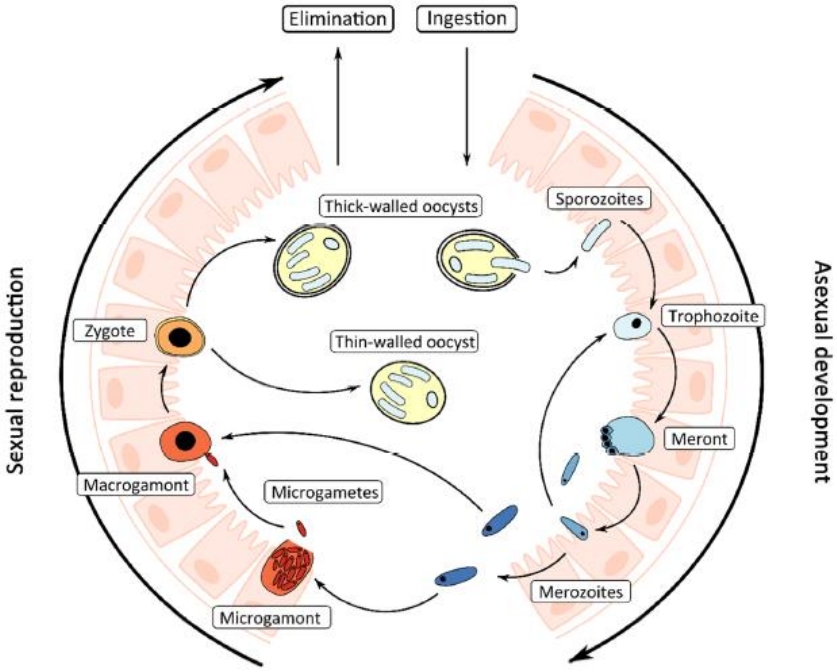

Figure 1.1 Schematic diagram of the asexual and sexual phases of the life cycle of *Cryptosporidium*. Used as is from [6].

Macrogamonts bud off microgametes that fertilize the microgamont to produce the zygote, the only diploid stage in the life cycle. The zygote develops into an oocyst which detaches from the enterocyte and sporulates during passage through the intestines [2]. Around 80% of the oocysts are thick-walled and are excreted to infect the next host, while 20% are thin-walled and release their sporozoites to infect additional enterocytes [9]. The recycling of the asexual stage and endogenous reinfection by thin-walled oocysts results in high parasitic levels and ensures high output of infectious thick-walled oocysts into the environment.

1.3 Symptoms and pathophysiology

Cryptosporidiosis most often presents as an acute infection that resolves within 2 weeks. Recurrent acute infections are common in immunocompromised patients, where brief periods of recovery are followed by disease remission [2]. Asymptomatic infection is estimated to constitute a significant percentage of cases, but, unsurprisingly, such infections are reported infrequently. Cryptosporidiosis

predominantly presents as watery diarrhoea which can be accompanied by nausea, abdominal cramps, vomiting and low-grade fever [3]. Although cryptosporidiosis is most commonly a disease of the small intestines and proximal colon, infection has been identified in the hepatobiliary system, extraintestinal gastric tract and even the respiratory tract in immunodeficient hosts.

The characteristic clinical presentation of watery diarrhoea results from sodium malabsorption, electrogenic chloride secretion and increased intestinal epithelial permeability [3]. Altered permeability is accompanied by decreased absorption of fluids and electrolytes, and is correlated to the severity of disease in children and AIDs patients [10]. Studies suggest that childhood *Cryptosporidium* infection, whether symptomatic or asymptomatic, is linked to malnutrition and growth retardation that may be caused by inflammatory damage to the small intestine [11]. Infection of the intestinal epithelial cells causes activation of nuclear factor-kB, which leads to the upregulation of a proinflammatory cascade that results in mucus hypersecretion, epithelial damage and loss of villous surface [12].

1.4 Diagnosis

As most clinical cases of cryptosporidiosis involve the gastrointestinal tract, diagnosis is usually through detection of shed oocysts or *Cryptosporidium* antigens in a single stool sample. Traditionally, microscopic identification of oocysts is used, and concentration methods such as formalin-ethyl acetate concentration or sugar solution flotation may aid diagnosis by improving oocyst yield and removing faecal debris [13]. Modified acid-fast staining is a cost-effective method often used to stain oocysts, however it is insensitive and requires high oocyst concentrations and interpretation by an experienced laboratory technician [14].

Direct immunofluorescence assays (DFA) utilize fluorescently labelled monoclonal antibodies (mAbs) targeting oocyst cell wall antigens and are up to 10 times more sensitive than acid-fast staining. Many commercial DFA kits such as the Meridian Bioscience DFA are available for diagnostics, and often are designed for codetection of *Giardia duodenalis*. Antigen detection by enzyme-linked immunosorbent assays (ELISA) or immunochromatographic tests are increasingly used for *Cryptosporidium* diagnosis as they do not require microscopic

identification and demonstrate high sensitivity, however, false positives and negatives are common [15].

1.5 Treatment

Management of cryptosporidiosis is usually supportive therapy focused on liquid and electrolyte replacement by the oral or intravenous route. Stool volumes in AIDs patients can exceed 10 L/d, and management of such severe diarrhoea requires intensive rehydration and electrolyte repletion. Diarrhoea can be treated with antimotility agents such as loperamide and diphenoxylate, and nutritional support by enteral or parenteral nutrition may be necessary if malabsorption is severe. As diarrhoea can result in lactase deficiency, supportive care should include a lactose-free diet.

In the case of HIV/AIDs patients with severe immune suppression and chronic cryptosporidiosis, antiretroviral therapy (ART) with immune restoration to a CD4 count >100/mm^3 usually results in drastic improvement and clinical resolution of disease [16]. It is recommended that ART should include an antiretroviral aspartyl protease inhibitor, as protease inhibitors have shown anti-cryptosporidial activity in vitro and animal models [17]. It must be considered that HIV/AIDs patients who appear to be cleared of infection tend to relapse if their CD4 counts decline, indicating that immune reconstitution may be essential for complete resolution in these patient groups.

The broad-spectrum antiparasitic nitazoxanide is the only pharmaceutical agent that is FDA-approved for the treatment of cryptosporidiosis in immunocompetent children and adults. Two randomized trials administered nitazoxanide 500 mg twice daily to HIV-negative adults over a 3-day duration, resulting in high person-to-person rates of disease resolution than placebo [18], [19]. Studies focused on HIV-positive cryptosporidiosis patients have shown no significant benefit of nitazoxanide alone on clinical outcomes. A study in Zambia of chronic cryptosporidiosis in malnourished children showed a decreased duration of diarrhoea and a decreased mortality rate in HIV-negative children, and no significant difference in clinical response or mortality in HIV-positive children [20]. A randomized trial in Mexico of nitazoxanide use in HIV-positive patients

suggested a correlation between nitazoxanide efficacy and CD4 count, where only patients who had CD4 counts >50/mm^3 responded positively to nitazoxanide treatment in comparison to placebo [21]. Hence, nitazoxanide treatment may be indicated in conjunction with ART, but never instead or without ART.

1.6 Modes of transmission

Transmission of *Cryptosporidium* occurs mainly through the faecal-oral route via ingestion of contaminated water or foods, direct person-to-person contact or zoonotic spread [9]. Studies have shown that most drinking water sources are contaminated by oocysts before treatment, and contaminated drinking water from surface or ground waters has been attributed to most major outbreaks of cryptosporidiosis [3]. Sewage contamination, failed water treatment and leakage into distribution systems are potential causes of such outbreaks. The largest recorded waterborne cryptosporidiosis outbreak occurred in Milwaukee, Wisconsin in 1993 where 403 000 people from a potentially exposed population of 1.6 million were affected and at least 54 died [22]. The causative species of the Milwaukee outbreak was *C. hominis*, but *C. parvum* has been associated with other waterborne outbreaks due to water contamination with agricultural runoff.

Contaminated recreational water is also associated with outbreaks of cryptosporidiosis. Public swimming pools have particularly been identified as a risk factor as chlorine concentrations of 1-3ppm recommended by Centres for Disease Control and Prevention are insufficient to disinfect water from environmentally hardy oocysts [3]. Foodborne cryptosporidiosis is rarely reported, but contamination has been documented from food sources such as raw produce, shellfish, apple cider and unpasteurized milk. Direct person-to-person contact is common, and outbreaks are commonly nosocomial or associated with day care centres or household spread. Zoonotic transmission is possible and domestic animals may be important reservoirs of human infection as a wider species diversity of *Cryptosporidium* has been recorded in rural areas with greater exposure to livestock and feral animals [2]. Furthermore, restricted animal contact has been shown to be correlated with a decrease in human cryptosporidiosis, demonstrated by the 2001 foot-and-mouth disease epidemic in the United Kingdom [23].

1.7 Global trends and outcomes

Cryptosporidium is a ubiquitous intestinal parasite with global distribution, and cryptosporidiosis infection has been reported in over 70 countries [24]. At least 44 species of *Cryptosporidium* exist, and of these over 19 species and genotypes have been reported in humans. Cryptosporidiosis is substantially underdiagnosed, and the global burden of disease is not yet well understood. Even in countries such as the USA, where the standardised *Cryptosporidium* EPA method 1623 was developed and modern diagnostics are readily available, it is estimated that only 1% of cases are diagnosed and reported [25]. A recent meta-analysis study on the global burden of *Cryptosporidium* identified that high-income countries have the lowest prevalence of infection, and that prevalence is significantly lower in urban areas regardless of national income due to better hygiene and access to treated water [24].

Cryptosporidiosis is associated with greater childhood morbidity and mortality than diarrhoeal disease from other causes, and younger ages are associated with higher risk of infection [4]. The Global Enteric Multicentre Study investigated the burden of paediatric diarrhoeal disease in sub-Saharan Africa and estimated that 2.9 million *Cryptosporidium* cases occur annually in children under the age of 2 years, and that mortality is increased two-fold in children aged between 1-2 years [5]. HIV status is an important risk factor for the host, and HIV-positive children are more likely to have *Cryptosporidium* infection than HIV-negative children [26].

1.8 Trends in South Africa

Cryptosporidium infection is common in South Africa and genotyping studies have shown that *C. hominis* is the most commonly detected species in humans in the country, followed by *C. parvum* and *C. meleagridis* [26]. The prevalence of *Cryptosporidiosis* has been described in several studies in the Limpopo, Kwa-Zulu Natal and Eastern Cape provinces and indicates high incidence rates in HIV-positive patients and children. A seroepidemiological study in HIV-infected adults and student volunteers in Limpopo found a seroprevalence of anti-*Cryptosporidium* IgG of 75.3% and 32.8% respectively [27]. In a separate study, screening of stool samples collected from patients attending an HIV treatment centre in Limpopo identified *Cryptosporidium* spp. in 35% of patients and interestingly, 39% of non-

diarrhoeal samples were positive for oocysts. These results are in accordance with the high endemicity of *Cryptosporidium* in HIV patients and in the region suggested in the previous study.

Environmental and demographic risk factors for *Cryptosporidium* infection were assessed in the Alice district in the Eastern Cape, and statistically significant risk factors were found to be lower socioeconomic status and contact with domestic animals [28]. Poor patient outcomes have been documented for cryptosporidiosis in children in South Africa. A study by Moodley et al. documented a 9% prevalence of *Cryptosporidium* in paediatric gastro-enteritis patients at King Edward VIII Hospital, 89.7% of whom were under 2 years of age [29]. From the cohort, 10% of infected children died and gastro-enteritis was confirmed as the cause of death for 6.3%. In a sequence diversity study of *Cryptosporidium* isolates in HIV-positive children admitted to the same hospital, 7 of 22 patients died 8 weeks post-admission [30].

South Africa is a water-scarce country, and as 14% of total freshwater stems from return flows such as treated sewage, inadequate purification processes account for significant freshwater pollution [31]. *Cryptosporidium* oocysts have been reported in multiple water sources such as raw sewage, treated effluent, and surface and drinking waters [32]. Dungeni and Mbomba assessed the prevalence of oocysts in four wastewater treatment plants in Gauteng and discovered that the mean removal efficiency of *Cryptosporidium* ranged between 67.40% and 98.26%, identifying the failure in effective removal of oocysts by South African wastewater treatment works [33]. The oocyst concentration from these effluents was greater than 1 oocyst/L, indicating a high risk of oocyst discharge into receiving water bodies that could potentially cause parasitic infection after exposure to these water sources. High removal efficiency was demonstrated only in the Zeekoegat Water Care Works, linked to effective physical processes incorporated into the plant. These findings stress the importance of upgrading wastewater treatment plants and conducting extensive testing to prevent waterborne outbreaks in a country like South Africa with high HIV endemicity.

It must be noted that in many waterborne outbreaks, water quality complied with the current microbiological standards of the country [34]. This is due to the persistence of *Cryptosporidium* oocysts in the absence of faecal indicator organisms such as *Escherichia coli* after chlorination processes, prompting the inclusion of *Cryptosporidium* testing in water safety guidelines. Therefore, the South African National Standard for drinking water, SANS241:2015, stipulates a standard limit of 0 oocysts/10L [35]. As the infectious dose of *Cryptosporidium* is low and oocysts occur in low numbers in aquatic environments, sampling such high volumes for oocyst detection is imperative despite necessitating cumbersome concentration methods for sample preparation.

1.9 Problem statement

Cryptosporidium infection causes significant morbidity and mortality throughout the world, but particularly in low-income countries such as South Africa. As no effective treatments for cryptosporidiosis are available for immunosuppressed patients, it is paramount that the focus shifts from treatment to disease prevention. *Cryptosporidium* is most commonly transmitted through contaminated drinking waters, and it is imperative that water sources are tested for the presence of this pathogen. However, routine testing of water for *Cryptosporidium* is currently inadequate and underused due to the high cost, low sensitivity and labour intensity of currently available testing methods. Immunosensors are an innovative, versatile, and adaptable option that are candidates to provide the highly sensitive, rapid, on-site analysis needed for *Cryptosporidium* detection in low-resource settings.

1.10 Aims and objectives

The aim of this study is the fabrication of a simple immunosensor for detection of the waterborne parasite *Cryptosporidium*. Gold nanoparticles will be synthesized and incorporated into the immunosensor design, enhancing the sensitivity of the sensor and serving as an immobilization platform for anti-*Cryptosporidium* capture antibodies.

1.10.1 Objectives

- Synthesis of gold nanoparticles using the Turkevich method.
- Characterization of their morphology and functionality using UV-Vis spectroscopy, dynamic light scattering, atomic force microscopy, transmission electron microscopy, energy-dispersive X-ray spectroscopy and cyclic voltammetry.
- Fabrication of a gold nanoparticle-based electrochemical immunosensor for detection of *Cryptosporidium*
- Optimization of detection of *Cryptosporidium* using cyclic voltammetry.

2. Chapter 2: Detection of *Cryptosporidium*

This chapter provides a literature review of the conventional methods used to detect *Cryptosporidium* and details the failure of these methods to enable sensitive, convenient and accurate analysis of water samples for this parasite. The shift to biosensors for *Cryptosporidium* detection is described by reviewing the biosensors that have been fabricated for this purpose. A brief overview of nanotechnology and gold nanoparticles as potential tools in biosensor development is included.

2.1 Conventional testing methods

A variety of technologies and methods are available for *Cryptosporidium* detection in water sources. Currently, the gold standard is the US EPA Method 1623 [36], which can be divided into four steps: 1) filtration or continuous flow centrifugation of at least 10L of water 2) separation of oocysts by immunomagnetic separation (IMS); 3) staining with fluorescently labelled antibodies and 4',6-diamidino-2-phenylindole (DAPI) and 4) fluorescence microscopy. For filtration, a cartridge or membrane filter can be used to concentrate oocysts, and portable pump and filter systems are available for in-field processing. Oocysts are eluted from the filter with an elution buffer through a mechanical wash process and recovery efficiencies (0-93%) have been shown to vary with the type and pore size of the filter membrane used, as well as the type of elution buffer [37].

Raw water typically contains a high number of undesired particles that are retained on the filter along with the oocysts such as soil, bacteria, algae, and other protozoans. This necessitates the use of IMS to purify eluted oocysts, reducing the number of false positives due to background particles. IMS kits like the Dynabeads® anti-*Cryptosporidium* kit contain super-paramagnetic beads functionalized with anti-*Cryptosporidium* mAbs that bind oocysts and can be separated by a magnet [38].

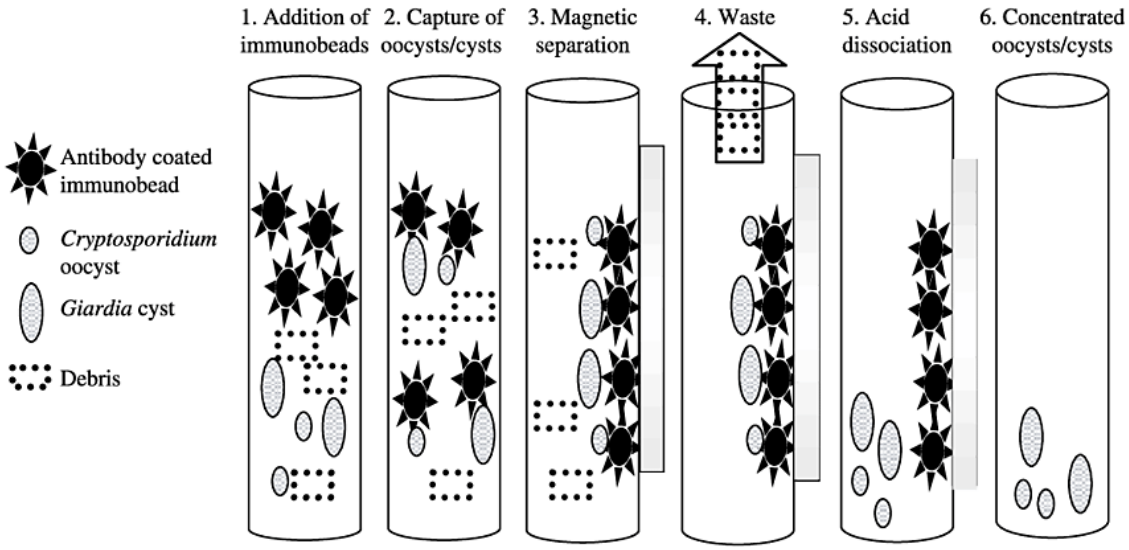

Figure 2.1: Schematic of the experimental steps in the immunomagnetic separation process of waterborne *Cryptosporidium.* Used as is from [39].

The purified oocysts are stained with approved fluorescently labelled anti-*Cryptosporidium* mAbs (MeriFluor® Cryptosporidium; Aqua-Glo™ G; Crypt-a-Glo™; EasyStain™C&G) and DAPI and enumerated by fluorescent microscopy and differential interference contrast (DIC) microscopy [36]. The EPA 1623 procedure is most commonly used in water analysis, however steps in the EPA method can be substituted by a variety of alternative technologies to enhance sensitivity, allow for species subtyping, or to reduce labour and costs [40]. Although the EPA procedure is most commonly used, the detection step is often achieved using alternative methods.

2.1.1 Microscopy-based

Microscopy-based methods have traditionally been relied on for detection of oocysts, however, there are few distinguishing morphological characteristics for *Cryptosporidium* and identification by light microscopy is unreliable [41]. Staining techniques can be employed to aid in differentiation of oocyst from other protozoa and environmental debris, the most popular of which is the acid-fast stain, also known as the Ziehl-Neelsen stain [42]. Although staining techniques are useful for oocyst detection, particularly in clinical applications, there are many limitations such as lack of specificity and sensitivity, and variability in stain uptake.

Additionally, some staining methods like malachite green or light green perbromide are time-consuming and require an experienced microscopist for reliable oocyst identification [14]. Phase contrast and DIC are microscopy methods that have been used to improve visualization and identification in comparison to light microscopy. These techniques provide higher contrast between the specimen and background and aid in revealing internal parasite morphology and have been incorporated into the US EPA 1623 method alongside immunofluorescence assay [40].

2.1.2 Immunology-based

Immunological assays for *Cryptosporidium* detection were developed to overcome the limitations of microscopy-based methods. The direct fluorescent antibody (DFA) assay uses fluorescein isothiocyanate-conjugated anti-*Cryptosporidium* monoclonal antibodies (FITC-C-mAb) that recognize surface epitopes on oocysts, and has demonstrated high specificities (96-100%) and sensitivities (98.5-100%) in environmental samples [14]. Nucleophilic fluorescent dyes such as DAPI and propidium iodide are often used in conjunction with DFA, as they actively stain sporozoite nuclei and facilitate morphological identification [43].

The specificity and sensitivity of monoclonal antibody-based DFA assays are influenced by various factors, including the purity of the *Cryptosporidium* antigen used to produce the mAb, the avidity and class/subclass of the antibody, the fluorochrome conjugated to the mAb and the detection system [43], [44], [45]. Studies have reported that IgG_1 isotype antibodies demonstrate better diagnostic specificity and increased avidity to oocyst surface antigens than IgG_3 or IgM for *Cryptosporidium* in water samples [46], [47]. A limitation to DFA and other immunoassays for *Cryptosporidium* is that commercially produced anti-*Cryptosporidium* mAbs are raised against a limited pool of *C. parvum* isolates, and significant variations in binding affinity may occur to different species or genotypes. Furthermore, the species or genotype of *Cryptosporidium* cannot be determined by DFA.

In contrast to DFA, indirect immunofluorescence assays require a primary and secondary antibody. The primary antibody is unconjugated and binds to the oocyst and the secondary fluorophore-conjugated antibody acts against the primary

antibody to enable detection. DFA is generally preferred to the indirect assay as only one tagging step is required, reducing processing time. Additionally, more non-specific binding and higher background is associated with the indirect assay as a result of using a second antibody [48].

Another strategy is enzyme-linked immunosorbent assay (ELISA), where an antibody against *Cryptosporidium* is immobilised on a 96-well plate surface. The sample is introduced, and enzyme-labelled secondary antibodies and substrate are added to enable colourimetric detection by absorbance spectroscopy. ELISA is predominantly used for detection of *Cryptosporidium* in stool samples but is not employed in water samples as water matrices are complex and the concentration of oocysts may be too low for detection [48]. Immunochromatographic lateral-flow assays have been developed for rapid detection of *Cryptosporidium* in faecal and water samples and are used frequently due to their simplicity, cost-effectiveness and rapid detection times. In this method, anti-*Cryptosporidium* antibodies are immobilized on a paper-based strip, and the sample is applied to migrate across the strip through capillary action, binding to the immobilized antibody.

Table 2.1 Comparison of conventional methods of detection of *Cryptosporidium* in water.

Method	**Principle**	**Advantages**	**Disadvantages**
Microscopy	Morphological identification aided by staining e.g., acid-fast, malachite green	Inexpensive, simple sample prep	Unreliable, time-consuming, require experienced personnel
Direct fluorescent antibody assay	FITC conjugated anti-*Cryptosporidium* mAbs	Increased specificity and sensitivity	Variations in binding affinity to different species, cannot determine genotype
Lateral flow assay	Test strip with immobilized anti-*Cryptosporidium* mAb	Simple, cost-effective, rapid detection	Low sensitivity
ELISA	Immobilized anti-*Cryptosporidium* antibody, enzyme-labelled secondary antibodies	Specificity, high throughput	Low sensitivity and susceptibility to background interference (water samples), time-consuming (multiple binding steps)
Molecular (PCR, LAMP)	Amplification of target DNA sequence	Specificity, allows for determination of genotype	Time-consuming, expensive equipment, requires trained personnel, oocyst lysis step

2.2 Existing biosensors for *Cryptosporidium* detection

As most current analytical methods for *Cryptosporidium* detection are costly, time-consuming and require specialized equipment, an urgent need exists to develop user-friendly, rapid testing platforms to detect *Cryptosporidium* species in water sources. Biosensors are analytical devices that can possibly overcome the drawbacks of conventional testing methods due to their sensitivity, sensitivity, cost-effectiveness and real-time analysis capabilities. Biosensors are composed of a biological receptor, transducer and detector. The biological receptor interacts with the analyte to generate a signal, a process known as bio-recognition, and the transducer transforms the bio-recognition event into a measurable signal which is measured by a suitable detector. Over the past 20 years, notable advancements have been made in *Cryptosporidium* biosensing, although refinement of these techniques is essential before their implementation in routine testing becomes viable. Several *Cryptosporidium* biosensors have been proposed and are summarized according to their signal transduction mechanisms.

2.2.1 Electrochemical

Electrochemical biosensors function by reacting with a target analyte to produce an electrical signal and are usually composed of a three-electrode system. Thiruppathiraja et al. developed an electrochemical enzyme amplified sandwich immunosensor using dual labelled gold nanoparticles and indium tin oxide (ITO) as the electrode for *C. parvum* detection [49]. An anti-oocyst monoclonal antibody was immobilized on a gold nanoparticle functionalized ITO electrode for oocyst capture, and a gold nanoparticle probe labelled with alkaline phosphatase and anti-oocyst Mab used for detection. Differential pulse voltammetry was used to measure the electrochemical signal, and a limit of detection of 3 oocysts/mL was achieved by the gold probe signal amplification system.

Aptamers are promising bioreceptors due to their high affinity and offer higher stability, longer shelf lives and lower production costs when compared to antibodies and have been widely used in electrochemical sensors. Iqbal et al. developed the first electrochemical aptasensor for *C. parvum* detection in fresh produce, a rapid label-free system with a detection limit of around 100 oocysts/30µl [50]. The

sensing interface consisted of a self-assembled monolayer of thiolated-DNA capture probe and anti-*C. parvum* aptamer on an AuNP-modified screen-printed carbon electrode. The redox current increase after oocyst to aptamer binding was measured by square wave voltammetry.

The same research group expanded on this work in spiked water matrices, fabricating an electrochemical aptasensor where biotinylated aptamer was bound to streptavidin-coated magnetic beads incorporated into an AuNP-modified screen-printed carbon electrode [51]. Square wave voltammetry was used to measure the increase in current, and the sensitivity of the aptasensor was greater than the first system, with an LOD of 50 oocysts/50µl in the buffer. However, oocysts at this LOD generated a lower change in current intensity than the signal for *G. duodenalis* in selectivity testing, even with 3 rounds of negative SELEX against *G. duodenalis* in the aptamer selection process [50]. Additionally, oocyst detection in raw water samples was assessed against a buffer blank and not compared to the unspiked water. Moreover, the LOD was not determined in a spiked water matrix. There is hence insufficient evidence to demonstrate that non-specific binding of contaminants does not occur in these matrices, and although aptamers may be an exciting prospect for whole oocyst detection considerable refinement of such systems is necessary.

Cryptosporidium oocysts produce the protein hsp70 in response to heat shock, and the mRNA gene coding for hsp70 is often used as a marker in nucleic-acid based detection methods [52]. Nugen et al. developed a polymethyl methacrylate (PMMA) chip-based electrochemical biosensor for detection of *Cryptosporidium* nucleic acids [53]. Standard photolithography was used to fabricate an interdigitated ultramicroelectrode array on the PMMA surface, and the analyte used was hsp70 mRNA extracted and amplified from *C. parvum* oocysts. The detection system was a sandwich hybridization assay based on a magnetic bead/liposome complex captured on the channel by a magnet. The capture probe was coated with superparamagnetic beads and the reporter probe was composed of liposomes entrapping potassium ferro/ferrihexacyanide, allowing for amperometric detection of the nucleic acids. The system was highly sensitive and enabled detection of amplified mRNA from a single oocyst, however, the method does not offer a

significant improvement over conventional methods due to expensive labels and the time-consuming preparation, mRNA extraction and amplification steps.

2.2.2 Raman Spectroscopy

Raman spectroscopy is a light scattering technique where incident monochromatic light is used to excite molecules to higher vibrational energy levels to emit radiation at a different wavelength, a process called Raman scattering. Raman signals are relatively weak and are enhanced by coating the sensing surface with noble metals. This technique is called Surface Enhanced Raman Spectroscopy (SERS), and when coupled to resonance enhancement by adjusting the incident light energy to the molecule electronic transition level, it is named Surface Enhanced Resonance Raman Spectroscopy (SERRS) [52].

Grow et al. reported the first label-free SERRS chip-based biosensor for *Cryptosporidium* detection, composed of a charge-coupled device array, surface-enhanced biochip and software for analysis [54]. The sensor was reported to theoretically detect a single oocyst, but no LOD was reported due to the low capture efficiency of the system. Rule and Vikesland developed a SERRS biosensor for co-detection of *C. parvum* and *G. lamblia* using immunogold Raman labels [55]. The labels were composed of gold nanoparticles conjugated to commercial monoclonal antibodies labelled with rhodamine B isothiocyanate and malachite green isothiocyanate respectively. The sensor specificity and sensitivity were high with no cross-reaction of antibodies, demonstrating the feasibility of a Raman-based method for multi-pathogen detection.

Many drawbacks exist to SERRS-based biosensors that limit their viability in *Cryptosporidium* analysis. Reproducible and quantitative analyses are a challenge, and no *Cryptosporidium* studies reported accurate detection limits [56]. The acquisition time is long, taking up to 15-20 min per oocyst and only highly concentrated low-volume samples can be analysed in a single step. Furthermore, oocysts need to be anchored to the surface as movement in the sample over the detection surface can disrupt measurements [52].

2.2.3 Surface Plasmon Resonance

Surface plasmon resonance (SPR) measures changes in refractive index at the interface between a dielectric material and planar metal surface. Bio-recognition is detected by coupling photons from a light source to surface plasmons and measuring the change in the incident and reflected light after analyte binding. Kang et al. have reported the use of an SPR biosensor with *C. parvum* as an analyte [57]. The system was a flow-type biosensor based on a mixed self-assembled monolayer, and a streptavidin interaction used to immobilize biotinylated anti-*C. parvum* monoclonal antibodies to the surface. Due to the low capture efficiency of the surface-immobilized antibody, the LOD was $1x10^6$ oocysts/mL. The sensitivity was enhanced to an LOD of 100 oocysts/mL by instead labelling the oocysts with biotinylated antibodies, taking advantage of the high-affinity reaction between the immobilized streptavidin and biotin. A drawback to this method is that the sample processing requires centrifugation, making it difficult to integrate the detection method into a continuous flow system. The biosensor was tested in a follow-up study in various buffer solutions, tap water and reservoir water [58], but only an unspiked buffer was used as a control. As variations in the refractive index of various sample matrices due to differing turbidity will influence the response of the system [52], these factors must at least be controlled for. However, an ideal system for SPR biosensing would include a processing step such as IMS purification to reduce complex matrix effects.

2.2.4 Cantilever

In cantilever-based sensors, binding of the analyte to an antibody-immobilized cantilever results in a decrease in resonance frequency corresponding to the increase in mass. This technique is suitable for targets heavier than molecular targets such as microorganisms that can generate significant signal changes [59]. Piezoelectric-excited millimetre-sized cantilevers (PEMC) are composed of two layers, a piezoelectric layer that acts as an actuator and sensor and a silica or glass layer that is functionalized with a receptor to bind the microorganism. Campbell and Mutharasan fabricated a PEMC IgM antibody functionalized biosensor that could detect *C. parvum* oocysts at 100 oocysts/mL [60]. A study by the same group

assessed detection of *C. parvum* by the PEMC biosensor in deionised water, PBS and milk [61], but testing in raw and drinking water matrices has not been performed.

2.2.5 Colourimetric/fluorescence

Colourimetric and fluorescent biosensors measure the colour or fluorescent signal produced by the biological recognition event, which can be seen by the naked eye or quantified using a simple optical instrument. Esch et al. developed a competitive lateral flow chip for detection of amplified hsp70 coding mRNA [62]. Amplicons were hybridized with dye-loaded liposomes conjugated to an oligonucleotide probe and biotin and loaded onto a nitrocellulose test strip. A probe complementary to the reporter was immobilized on the control zone, and anti-biotin antibody immobilized on the test zone where liposomes would bind in the presence of target mRNA. The same group developed a similar microfluidic fluorescence biosensor based on an mRNA-detecting sandwich assay [63]. Reporter probes were conjugated to carboxyfluorescein-loaded liposomes to enhance the detection signal. Both systems allowed for detection of low concentrations of the mRNA, and several studies have since reported lateral flow sensors for an hsp70 mRNA target. However, all experience the disadvantages of most nucleic acid-based sensors such as time-consuming pre-treatment and expensive reagents.

2.3 Nanotechnology

Nanoscience is a discipline of science and engineering concerned with the unique properties and phenomena associated with materials that exist at a nanometre scale. Nanomaterials are substances that are confined to the nanoscale in at least one dimension, between 1-100nm [64]. Nanotechnology is the construction and application of nanomaterials in medicine and devices and has immense potential to revolutionize science and modern society. The large surface-to-volume ratio and quantum effects of nanomaterials impart radically different properties in comparison to the bulk material. The nanomaterial surface becomes increasingly reactive at the nanoscale and exhibits catalytic and absorbance activities which can be utilized in a variety of different applications such as catalysis, purification, drug delivery and sensors.

Nanotechnology is becoming increasingly important in biosensor development due to its capacity to increase biosensor sensitivity and performance by several orders of magnitude [65]. Engineered nanomaterials have a higher electrical conductivity and can be used to amplify desired signals. They are also compatible with biological materials and can be conjugated to biomolecules such as enzymes, antibodies and DNA [66]. For the purposes of this study, gold nanoparticles were chosen as a candidate to incorporate into the immunosensor for signal enhancement and immobilization of the anti-*Cryptosporidium* antibody on the transducer surface of the sensor.

2.3.1 Gold nanoparticles and their applications in biosensors

Gold nanoparticles (AuNPs) have emerged as a promising candidate for labelling, imaging, sensing and drug delivery applications due to their unique size-dependent physicochemical properties and tuneable optical properties. AuNPs are prepared as a colloidal suspension, and the colloid is usually wine-coloured for spherical NPs under 100nm or blue/purple for large spherical particles or nanorods [66]. AuNPs are known to be highly stable and have been prepared in a variety of shapes and structures including nanospheres, nanocubes, nanocages, nanorods, nanoshells and nanoflowers (Figure 2.2) [67]. The surface of AuNPs can be modified to enhance their biocompatibility and functionality by the conjugation of biomolecules via physisorption or chemisorption.

The properties of AuNPs are of particular interest for applications such as molecular recognition, chemical sensing and imaging, and are highly suitable for incorporation into biosensors. Due to their unique optical properties, AuNPs are often used in optical biosensors to enhance the detection sensitivity of fluorescence, chemiluminescence, as SPR and SERS enhancers and as colourimetric markers [68]. AuNPs are also used in non-optical biosensors such as piezoelectric and electrochemical biosensors. The high density of AuNPs is utilized in piezoelectric biosensors as a label to increase the mass change and improve the frequency shift to enhance sensitivity [69]. In electrochemical biosensors, AuNPs are used as an immobilization platform, electrocatalyst, or an enhancer of electron migration to improve the electrochemical signal and improve sensitivity [70].

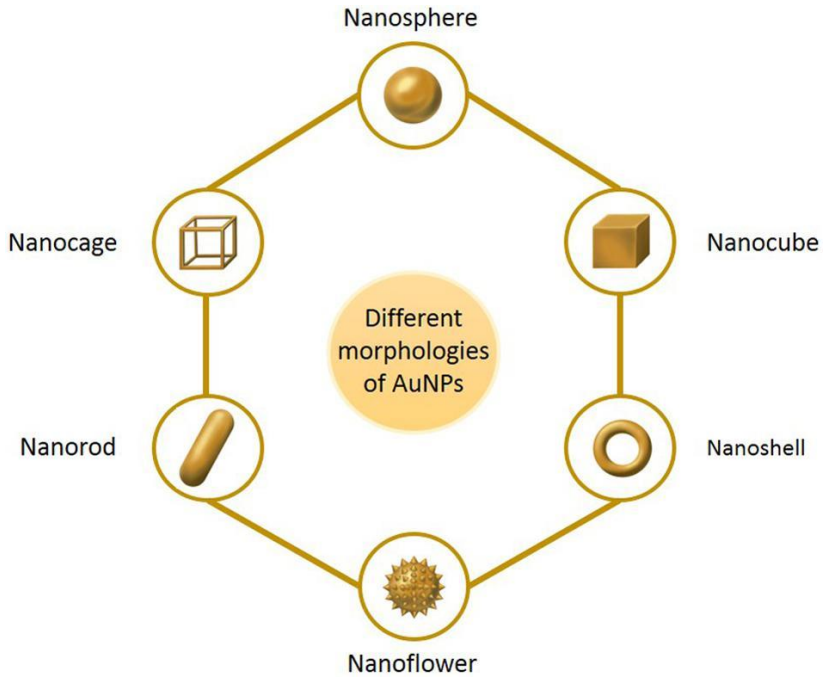

Figure 2.2: Schematic representing the main morphologies of gold nanoparticles. Used as is from [67].

The inherent redox ability of AuNPs due to the redox reaction of Au^0 and Au^{3+} makes them good candidates as electrochemical indicators. There are many strategies to detect the AuNPs electrochemical signal but the most common are: direct detection of the oxidation signal without treatment, electro-oxidation of AuNPs to gold ions in HCl solution and dissolving the AuNPs in HBr/Br_2 acidic solution [71]–[73].

Using AuNPs as electrochemical indicators has been utilized in several biosensors, but the most common use of AuNPs in biosensors is for electron migration enhancement. In an electrochemical biosensor, the redox reaction gives rise to electron exchange on the electrode relative to the analyte concentration. However, the weak electrical conductivity of biomolecules which are routinely used as biorecognition elements may block the transfer of electrons to the electrode. Additionally, the adsorption of biomolecules directly onto the naked surface of the electrode may result in denaturation and loss of activity [68]. The immobilization of AuNPs to the surface of the electrode enhances the conductivity to not only increase the electron transfer rate, but to also enlarge the sensing area and increase the amount of immobilized biorecognition element along with its bioactivity [70].

Immobilization of AuNPs on the surface of electrodes can be carried out using electrodeposition or simple direct immobilization through drop casting. The size of AuNPs has been shown to influence the performance of the biosensor by affecting the linearity of the output signal and reproducibility of the assay [70]. Furthermore, the large surface-specific surface area of small AuNPs results in the immobilization of a larger number of biomolecules, in turn enhancing sensitivity.

2.3.2 Synthesis of gold nanoparticles

Synthesis of AuNPs can be achieved using a variety of physical, chemical and biological synthesis methods. The synthesis of any nanoparticle can be grouped into two methods: the top-down approach or the bottom-up approach [74]. The top-down approach is based on the breaking down of bulk materials and subsequent stabilization of the nanoparticles by adding protecting agents. These approaches include micropatterning, photolithography, pyrolysis, lithography, thermolysis and radiation-induced methods [67]. Top-down approach methods are limited in the control of the structure and surface of AuNPs, making it difficult to control their physical and chemical properties. Most of these methods require high pressures and temperatures to synthesize the AuNPs and are uneconomical.

The bottom-up approach is the construction of a nanomaterial from atomic or molecular units and usually involves two stages: the reduction of an aqueous gold salt solution by a reducing agent, and the stabilization of the AuNPs by a capping agent to prevent agglomeration [74]. The most commonly used bottom-up method is chemical synthesis, involving the chemical reduction of $HAuCl_4$ to Au^0 atoms in solution. The Turkevich method is the one of the most popular techniques for formulation of spherical AuNPs, wherein sodium citrate is used simultaneously as a reducing agent and a capping agent (Figure 2.3). A solution of $HAuCl_4$ is heated to boiling temperatures and citrate ions are added to the solution rapidly under continuous stirring. The gold salt is reduced to AuNPs, and the excess of citrate ions associate with the surface of the AuNPs to impart a net negative charge and electrostatically repel other AuNPs to prevent agglomeration. The molar ratio of the reducing agent and the gold salt can be altered to produce spherical AuNPs within a size range of 10-150nm [75].

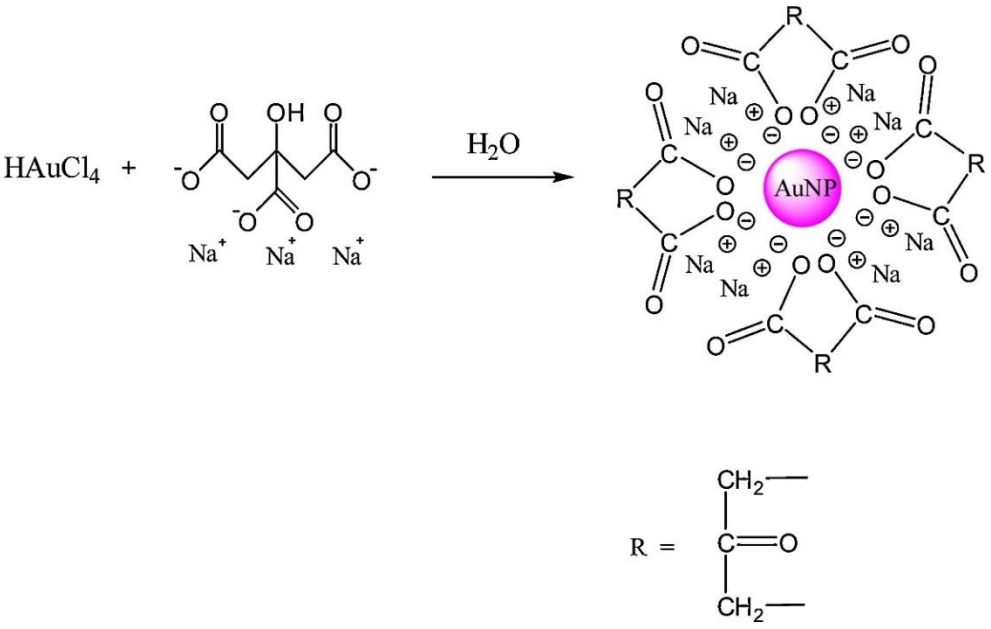

Figure 2.3 Schematic representing the reduction of gold salt to gold nanoparticles via the Turkevich method. Used as is from [76].

Another chemical synthesis method used to synthesize spherical AuNPs is the Brust method which uses a phase transfer to transfer gold salt to an organic solvent like toluene [64]. Thereafter, the gold is reduced with sodium borohydride along with an alkanethiol to stabilize the AuNPs. Techniques such as the seed-mediated growth method can be used to synthesize AuNPs with different geometries. Rod-shaped AuNPs are synthesized by first synthesizing seed particles by reduction of the gold salt by $NaBH_4$, and transferring the seed particles to a metal salt and weak reducing agent such as ascorbic acid to prevent further nucleation [77]. The shapes of the AuNPs depend on the concentration of the reducing agents and seeds.

Recently, biological synthesis methods have grown in popularity to offer a clean, bio-friendly alternative to the harsh chemical used in some chemical synthesis reactions. Biological reductants that have been used for AuNP synthesis range from bacterial and fungal cells, plant extracts, algae and biomolecules. Limitations of biological synthesis are long synthesis times as bacteria and fungi take days to culture, difficulty of identification of reactive compounds in plant biomass, and the lack of stability of AuNPs synthesized [74].

2.3.3 Functionalization of gold nanoparticles

AuNPs can be functionalized with a variety of biomolecules depending on their intended function. Attachment of biomolecules capable of specific target recognition allows for biorecognition in drug delivery, in vivo bioimaging and biosensors, and is referred to as bioconjugation. Physical and chemical interactions can be utilized for attachment of antibodies to the surface of AuNPs. Physical interactions include: ionic attractions between the positively charged antibody via the N-terminal or positively charged amino acids and the negatively charged AuNP, hydrophobic attractions between the antibody and surface of the AuNP, and dative binding between the conducting electrons of gold and the sulphur atoms of amino acid groups in the antibody [78]. Physisorption of antibodies to AuNPs is a simple and convenient option, however, several disadvantages exist. High concentrations of antibodies have to be used, and random orientation of antibodies limits their activity. Additionally, the binding is weak and easily altered by changes in pH, leading to replacement of the antibodies by other biomolecules in biological samples.

Chemical interactions between antibodies and AuNPs can be introduced via several methods that include: chemisorption via thiol derivatives, use of bifunctional linker molecules, and use of adapter molecules such as biotin and streptavidin [66]. A common method is introduction of functional groups to the AuNP surface and conversion of these groups to other functional groups by bifunctional molecules. Carboxylic moieties are reacted with primary amines via a condensation reaction to form amide bonds. Water-soluble carbodiimides such as 1-Ethyl-3-(3-dimethylaminopropyl)carbodiimide (EDC) are usually utilized for this step. After the intermediate compound is formed, the activated group is reactive toward primary amines, and an active ester compound such as N-hydroxy-succinimide (NHS) is utilized to form amide bonds [79].

3. Chapter 3: Methodology

In this chapter, the methods, materials and instrumentation used for the synthesis and characterization of the gold nanoparticles and fabrication of the immunosensor are presented. The principle of the characterization techniques and cyclic voltammetry is also described.

Table 3.1 Consumables list.

Reagent	Catalogue Number	Supplier
Trisodium citrate	A12274	Alfa Aesar
$HAuCl_4.3H_2O$	520918-1G	Sigma-Aldrich
Ferricyanide	2312118	Saarchem
KCl	5043680	Fluka
Anti-Cryptosporidium mouse monoclonal antibody [BEL 0126]	ab54066	Abcam
Oocysts heat inactivated	WBI-P102CC	Waterbourne Inc
Alumina polishing powder (1, 0.3, 0.05 µM)	406322016, 4010078,4010075	Buehler
Carbol fuschin	C4165-25G	Sigma-Aldrich

Table 3.2 Instrument and equipment list.

Equipment	Supplier
pH50 VioLab Benchtop pH meter	Lasec
UV/Vis 920	GBC Scientific
Nanosurf EasyScan 2 STM	Nanosurf
PointProbe® Plus SPM Probe Silicon Cantilever	Nanosensors™
Screen-printed carbon electrode	Metrohm Dropsens
10.00mm QS Cuvette	Hellma Analytics

Tecnai G220 Field High Resolution Transmission Electron Microscope	Electron Microscope Unit (EMU), UWC.
Malvern Zetasizer Nanoseries ZS90	MalvernPanalytical
PalmSens4 Potentiostat	PalmSens
Purite OndeoJS Water Purifier	Purite Ltd.

3.1 Synthesis of AuNPs

A standard citrate reduction method at a $Na_3C_6H_5O_7$/HAuCl4 molar ratio of 3.4:1 was used to synthesize the AuNPs [49], [80]. A 100 mL volume of 1mM HAuCl4.3H2O was heated to 100°C with vigorous stirring. An aliquot of 10mL 1% trisodium citrate was rapidly added to the vortex of the solution, resulting in a colour change from pale yellow to red. The solution was kept at 100°C for an additional 10 minutes, after which the heat was removed and stirring allowed to continue for another 15 minutes. The colloid was cooled to room temperature and the AuNPs were characterized and used for sensor applications.

3.2 Characterization of AuNPs

3.2.1. UV-Vis Spectroscopy

UV-Vis spectroscopy measures the amount of ultraviolet or visible light that is absorbed by or transmitted through a sample over a fixed path length in comparison to a reference or blank sample. UV-Vis spectroscopy is a useful method for characterization of gold nanoparticles in order to obtain an indication of the size and size distribution of the gold nanoparticles. The surface plasmon resonance of AuNPs results in a characteristic UV-Vis extinction spectrum dependent on the size, shape and aggregation of AuNPs [81].

The distinctive optical feature of AuNPs is referred to as localized surface plasmon resonance (LSPR) and is the collective oscillation of conduction band electrons in resonance with a characteristic wavelength of incident light [82]. The LSPR of AuNPs produces an intensely coloured solution with a strong absorption band in the visible region of 500-600nm, measurable by UV-Vis spectroscopy. An increase

in particle diameter results in a correspondent increase of the peak absorbance wavelength and a red shift of the absorbance spectrum [66]. This effect is also observed with unevenly shaped AuNPs, where a significant red shift is observed in the spectrum in comparison to spherical-shaped particles. The peak absorbance of the sample is linearly correlated to the concentration of AuNPs in the solution.

The UV-Vis spectrum of the AuNP solution was analyzed in a range of 300-800nm. A QS Cuvette with a pathlength of 1cm was used to measure the spectra on a UV/Vis 920 spectrophotometer. The AuNP solution was diluted in a 1:2 ratio with diH_2O to reduce background of the measurements, and deionized water was used as a blank. UV-Vis readings were taken immediately after synthesis of the AuNPs and weekly thereafter for one month to assess the stability of the nanoparticles. Raw data was obtained from the Cintral software and further analyzed.

3.2.2 Dynamic light scattering and zeta potential analysis

Dynamic light scattering (DLS) is a technique based on Brownian motion that is commonly used for characterizing the hydrodynamic radii of nanoparticles by defining their diffusion behaviour in solution [83]. Suspended NPs are in a state of constant collision with solvent molecules, resulting in energy transfer and inducing particle movement. This effect is more noticeable in small particles, and if all parameters which have an influence on the particle movement are fixed, the hydrodynamic diameter of the particles can be measured.

In a DLS instrument, a single-frequency laser is aimed at a colloidal solution in a cuvette and the incident laser light is scattered in different directions resulting in a signal used to determine the particle size. Another important parameter that a DLS instrument can measure is the polydispersity index (PDI). The PDI is the representation of the heterogeneity of the sample based on the size distribution and provides an indication of the extent of variability of particle size, shape and agglomeration of the NPs [84].

Zeta potential analysis provides an indicator of the potential stability of a nanoparticle colloidal solution. The surface charge of nanoparticles attracts a thin layer of ions with an opposite charge to the surface of the NP, and the zeta potential

is the measure of electric potential difference at the boundary of this double layer at the slipping plane [85]. The magnitude of the zeta potential indicates the degree of repulsion between similarly charged particles in dispersion. High absolute values of zeta potential will indicate good stability of the dispersed nanoparticles which resist aggregation and agglomeration over time. Generally, colloids with a high negative or positive zeta potential are electrically stabilized while colloids with a low zeta potential +- 5 mV will tend towards aggregation due to van der Waal forces dominating between particles. A zeta potential of +- 30 mV is generally regarded as highly stable [64].

Size, polydispersity index and zeta-potential measurements of the AuNPs were acquired on a Malvern Zetasizer Nanoseries ZS90. The readings were taken using a capillary cuvette and a quartz cuvette. An aliquot of the AuNP solution was diluted in a 1:10 ratio in diH_2O to obtain the measurements.

3.2.3 High resolution transmission electron microscopy (HRTEM)

Transmission electron microscopy (TEM) is a microscopy technique used to image NPs to obtain information on their size, grain size, size distribution and morphologies. The utilization of a particle beam of electrons enables a far greater resolution of specimens than a conventional optical microscope, resolving subjects as small as atomic structures.

The electron gun of the TEM unit emits electrons through the vacuum tube of the microscope, reaching an electromagnetic condenser lens which focuses the electrons into a fine beam transmitted through the thinly sectioned specimen. The electrons scatter and the objective lenses produce an intermediate magnified bright field image. The contrast in a TEM image is attributed to the electron-absorbing capability of the material dependent on the composition or thickness of the sample. Areas that fewer electrons were transmitted through appear darker, while lighter areas represent transmission of more electrons.

The morphology of the AuNPs was determined using an FEI Tecnai G2 F20 S-Twin HRTEM. The AuNP colloidal sample was pipetted onto a carbon-coated copper grid and allowed to dry under a Xenon lamp for 10 minutes. The sample

was imaged under brightfield mode conditions at a 200 kV accelerating voltage. Images obtained were analyzed with ImageJ Software.

3.2.4 Energy-dispersive x-ray spectroscopy

Energy-dispersive X-ray spectroscopy (EDX) is an analytical technique that enables the elemental analysis or chemical characterization of a sample. The technique is based on energy analysis of X-rays that are emitted by a material subjected to electromagnetic radiation. Every element has a unique atomic structure which creates a unique set of peaks on an electromagnetic emission spectrum and allows for its chemical characterization.

Atoms at rest contain ground-state electrons within discrete energy levels. In an EDX unit, a high energy beam is focused on a sample and the incident beam excites the ground state electron to eject from the shell and create an electron hole where the electron was located. An electron from a higher, outer energy level fills the hole, and the energy difference between the two levels is released as an X-ray. The number and energy of the X-rays emitted is measured by an energy-dispersive spectrometer and matched to the characteristic spectrum of a given element [86].

The elemental composition of the AuNPs was analyzed using an FEI Tecnai G2 F20 S-Twin HRTEM. The sample was prepared as described in section 3.2.3.

3.2.5 Atomic force microscopy

Atomic force microscopy (AFM) is a surface analysis technique utilizing scanning probe microscopy to achieve resolution at the nanoscale. The high resolution of AFM is suited for characterizing many physical properties of nanomaterials such as size, morphology, surface texture and roughness. An AFM system is composed of a sharp tip approximately 10-20nm in diameter attached to a Si or Si_3N_4 cantilever. This probe is raster-scanned over the surface of the sample, and the repulsive forces that dominate the interaction of the tip and the surface is measured by focusing a laser beam with a photodiode. Unlike an electron microscope, AFM provides a true 3D surface profile and no treatment or preparation of the sample is required for visualization [87].

The morphology of the AuNPs was determined using the Nanosurf EasyScan 2 STM. The AuNP colloidal solution was pipetted onto a glass slide, allowed to dry for 30 minutes and AFM data was acquired using continuous scan mode configuration.

3.3 Immunosensor fabrication and electrochemical detection of *Cryptosporidium*

Cyclic voltammetry (CV) was used to investigate the redox behaviour of the immunosensor system with the modified GCE at different stages of fabrication. CV is a linear potential sweep method for electrochemical analysis that monitors the redox behaviour of a chemical species within a set potential range. CV is based on measuring the current response to a linearly cycled potential between the working and the reference electrodes [88]. When the set potential limit is reached, the potential is scanned in the opposite direction back to the original potential to complete the cycle, resulting in the characteristic "duck-shaped" voltammogram in Figure 3.1, where the y-axis is the current response, and the x-axis is the applied potential to the system. The scan rate in CV is defined as the rate of change of potential over time.

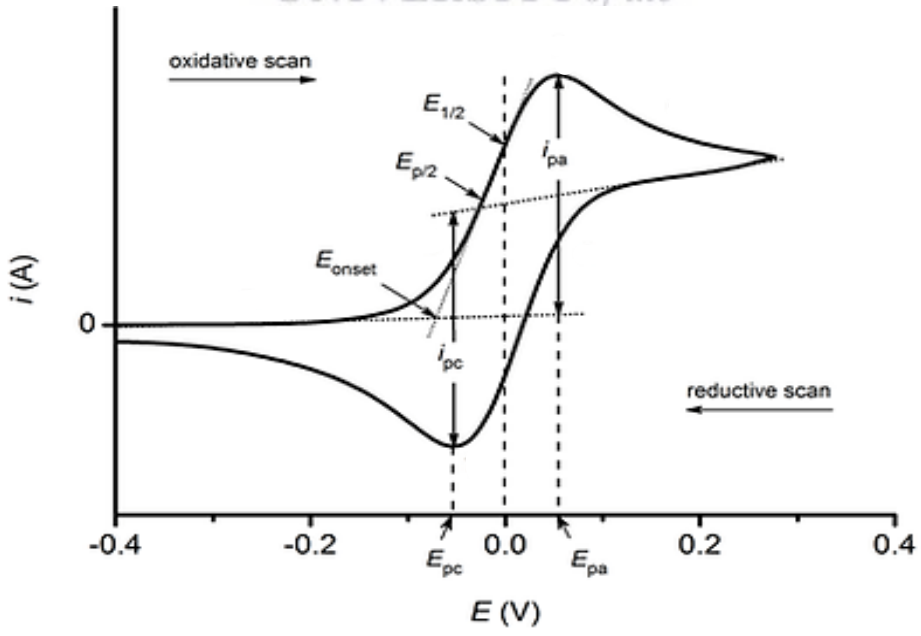

Figure 3.1 An example of a standard cyclic voltammogram for a reversible redox system. Adapted from [89].

In a reversible redox couple such as ferrocyanide/ferricyanide when the potential is scanned positively on the forward scan $Fe(CN)_6^{-4}$ is oxidized and the oxidation current increases to a peak. This is called the anodic peak current i_{pa} which occurs at the corresponding anodic peak potential E_{pa} [90] . The anodic current is therefore due to the electrode process of:

$$Fe(CN)_6^{-4} \rightarrow Fe(CN)_6^{-3} + e$$

When the scan direction is reversed, the potential is still sufficiently positive to oxidize the $Fe(CN)_6^{-4}$ and the anodic current continues, however when the applied potential is sufficiently strong enough to reduce the $Fe(CN)_6^{-3}$ the reduction current increases to a peak called the cathodic peak i_{pc} at the corresponding cathodic peak potential E_{pc}. The process at the electrode is:

$$Fe(CN)_6^{-3} + e \rightarrow Fe(CN)_6^{-4}$$

The cathodic and anodic peak currents provide information on important parameters such as reversibility, irreversibility and the rate of the electron transfer processes for the system. Redox couples where half reactions result in the rapid exchange of electrons at the working electrode are defined as electrochemically reversible couples. The formal reduction potential (E^o) is the mean of the E_{pa} and E_{pc} and is defined by the following equation:

$$E^o = \frac{Epa + Epc}{2}$$

In a reversible couple, the number of electrons involved in the redox reaction is defined by the difference in peak potentials:

$$E_{pa} - E_{pc} = \frac{59mV}{n}$$

The peak current in a reversible system is defined by the Randles-Sevcik equation below. The peak current increases with $v^{1/2}$ and is directly proportional to the concentration of the redox species. The i_{pa} ad i_{pc} values should be similar for a one-step reversible couple.

$$I_{pc} = 2.69x10^8 n^{3/2} A D^{1/2} v^{1/2} C$$

Where: i_{pc} = peak current A

n = # electrons involved

A = electrode area, m^2

D = diffusion coefficient, m^2/s

C = concentration mol/L

v = scan rate, V/s

The fabrication protocol of the immunosensor is shown in Figure 3.2 and is as follows; the GCE was polished with 1, 0.3 and 0.05µm alumina slurry on a polishing pad prior to surface modification of the electrode. The GCE was rinsed with ethanol and sonicated in ethanol and water consecutively for 15 minutes to remove any alumina residue. 5 µL of the AuNP solution was drop cast and allowed to dry on the surface of the GCE for 30 minutes at room temperature. The electrode was rinsed with diH_2O and 5 µL of the anti-*Cryptosporidium* mAb was drop cast on the surface of the GCE and allowed to dry for 30 minutes at room temperature.

Cyclic voltammetry experiments were carried out using a PalmSens4 Potentiostat. The modified working electrode was immersed in 1 mL of 5 mM ferricyanide in 0.1M KCl solution. The system was a three-electrode arrangement, using the modified glassy carbon electrode, an Ag/AgCl reference electrode, and a platinum counter electrode. A working solution of *C. parvum* oocysts was added to the electrolyte solution and the solution stirred using a magnetic stirrer for 30 seconds. The oocysts were incubated in the electrolyte solution for 5 minutes before a cyclic voltammetry measurement was taken at a potential range of -1.0-1.0 mV and a scan rate of 100 $mV.s^{-1}$.

The anti-*Cryptosporidium* mAb (1$mg.mL^{-1}$) was aliquoted and stored at -20°C immediately upon receipt. Aliquots were thawed and diluted to 100, 10 and 1 $\mu g.mL^{-1}$ in an antibody dilution buffer (0.01M phosphate-buffered saline, 0.1% bovine serum albumin pH 7.2). The heat-inactivated *Cryptosporidium* oocyst solution ($1.25x10^6$ $oocysts.mL^{-1}$) was stored at 8°C upon receipt, and serial

dilutions in 0.01M PBS were used to make up the working stock of 1000 oocysts.mL^{-1}.

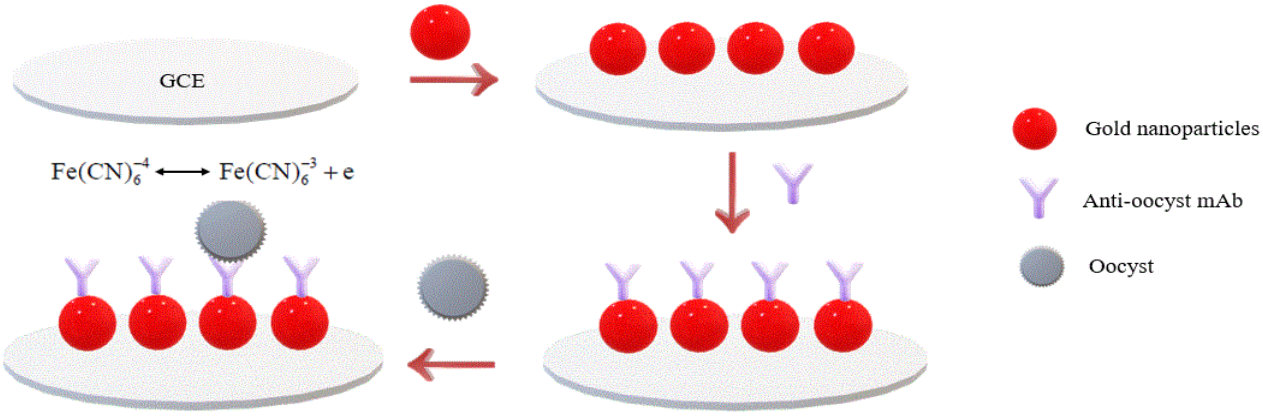

Figure 3.2 Schematic illustration of the fabrication process of the immunosensor

3.3.1 Scan rate study

The electrochemical behaviour of the modified GCE was characterized with a scan rate study to compare the difference in the electrochemical parameters of the ferricyanide/ferrocyanide redox couple at the interface of the GCE at varying stages of fabrication. The sensor was constructed as previously described with the exception of using an electrolyte volume of 3 mL, and cyclic voltammetry measurements were taken in a potential range of -1.0-1.0 mV at scan rates 10, 50, 100, 125, 150, 175 and 200 mV.s^{-1}. The bare GCE, AuNP-coated GCE and AuNP/anti-oocyst mAb-coated GCE were compared (at anti-oocyst mAb concentrations of 100, 10 and 1 µg.mL^{-1}).

3.3.2 Response time optimization

The sensor was set up as previously described and 100 oocysts were added to the ferricyanide solution and the response was measured after 30 seconds of stirring and 0, 5, 10, 15, 20, 25 and 30-minute time intervals.

3.3.3 Calibration of concentration response

The immunosensor was set up as previously described and increasing amounts of oocysts were added to the ferricyanide solution and the response was measured after 30 seconds of stirring. Different concentration ranges were evaluated to determine

a linear range of immunosensor response, at 0-10 oocyst.mL^{-1}, 0-100 oocyst.mL^{-1} and 0-1000 oocyst.mL^{-1}. The experiments were carried out in triplicate (n=3).

3.4 *Cryptosporidium* staining protocol

The presence of oocysts in the working stock used for the immunosensor calibration was confirmed using a modified Ziehl-Neelsen stain. The *Cryptosporidium* working stock was pipetted onto a glass slide and allowed to air dry. The specimen was fixed with 100% methanol for 3 minutes and stained with carbon fuchsin for 15-20 minutes. The specimen was rinsed thoroughly with tap water, decolourized with 1% HCl in ethanol and counterstained with methylene blue for 30 seconds. The glass slide was rinsed again with tap water, air dried and examined under x10 and x40 objectives.

4. Chapter 4: Results and Discussion

This chapter discusses the characterized morphology, chemical composition and stability of the synthesized gold nanoparticles. Furthermore, the fabrication, optimization and performance of the immunosensor are detailed, and the verification of the working stock of *Cryptosporidium* is described.

4.1 AuNP characterization

4.1.1. UV-Vis Spectroscopy

Figure 4.1 shows the UV-Vis spectrum of the synthesized citrate-capped AuNPs taken every week over the course of a month after synthesis. A broad absorbance peak is observed ranging from 500-600nm, with a peak absorbance wavelength of 525nm. Gold nanoparticles are known to have varying specific absorption spectra according to their size and shape, and when the diameter of AuNPs measures between 12-41nm the corresponding maximum absorption peak is located at 520-530nm [91]. This spectrum indicates that the majority of the AuNPs are located within this size range, however, the broadness of the peak suggests that the AuNP colloidal is heterogenous in size and possibly shape, with a variation in size broadening the absorbance peak.

When the diameter of AuNPs exceeds 41nm, a corresponding extinction spectrum shift occurs towards longer wavelengths, known as red shift. Hence, the absorbance at wavelengths larger than 600nm in Figure 4.1 indicates that some of the AuNPs in the sample are larger than 41nm or have irreversibly agglomerated. This was in accordance with the visual analysis of the sample in Figure 4.2, which appeared to be a reddish-purple colour instead of the expected orange-red colour.

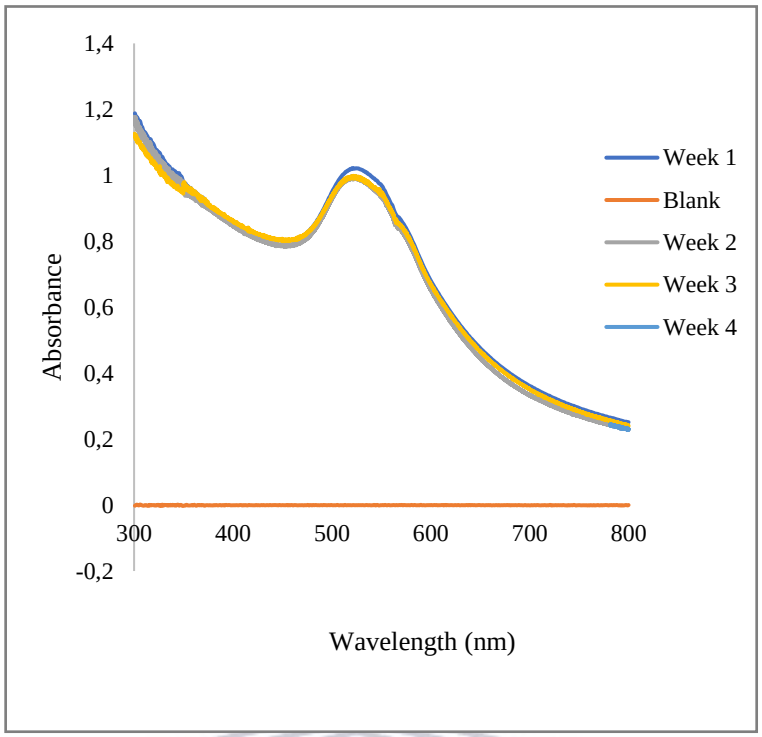

Figure 4.1 Absorbance spectrum of 1:2 dilution of AuNPs at various time points after synthesis.

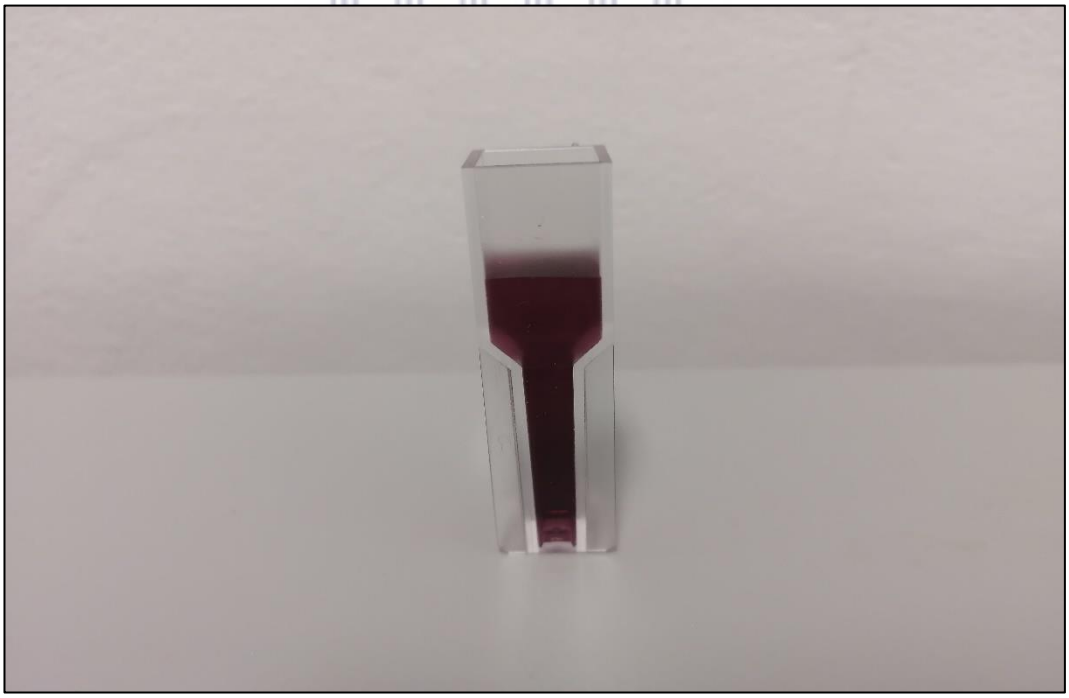

Figure 4.2: Wine red colour of synthesized AuNPs synthesized by the Turkevich method.

The Turkevich method is one of the most common methods for producing small, monodisperse spherical AuNPs [92], but the UV characterization results show that the synthesized AuNPs are polydisperse in nature. Studies have indicated that a larger citrate/gold molar ratio from 0:7:1 to 3.5:1 results in an increase in the number of nuclei and a reduced final AuNP size, while ratios beyond 3.5:1 result in a size of 30 nm [93]. As the molar ratio in this reaction was 3.4:1, this should not be a contributing factor to the size variation in the sample.

However, another factor that has been proven to be crucial for size control and the monodispersity of the AuNPs is the pH of the reaction mixture. Tyagi and colleagues investigated the role of pH at different molar ratios of citrate/gold and showed that each mole ratio had a specific optimal pH for a narrower size distribution, and that the initial pH value of the solution is one of the critical size deciding parameters of AuNPs [94]. The findings for the molar ratio 3:1 was that a pH of 3-4 was optimal for synthesis of AuNPs with a narrow size distribution, and a pH of 5 and above increased the polydispersity of the sample significantly. In this experiment, the pH of the reaction mixture was not measured before or during synthesis, and the pH was not a controlled variable. As sodium citrate is a weak base it is probable that the pH of the reaction mixture was above the optimal acidic pH described by Tyagi *et al.* for a similar molar ratio. Ideally, the AuNPs synthesized for this study should have been synthesized at various pH levels to obtain the optimal pH level for the synthesis of monodisperse AuNPs.

Although the AuNPs are not monodisperse, their stability over time was determined by monitoring the UV-Vis spectrum for a month. The decrease in absorbance at the maximum absorbance wavelength was minimal for weeks 2-4 in comparison to the beginning of week 1, indicating that the AuNPs were stable for at least a month after synthesis. The absorbance peak did not shift towards higher wavelengths, showing that the citrate ions were effective in stabilizing the AuNPs from agglomerating over time.

4.1.2 Dynamic light scattering

From the data in table 4.1, the size distribution conclusions in section 4.1.1 can be confirmed. Numerical values of PDI range from 0.0 to 1.0, with 0.0 indicating a perfectly uniform sample with respect to particle size while values close to 1 reveal a highly polydisperse sample containing multiple particle size populations [95]. A PDI value below 0.5 is considered to indicate a narrow size distribution, and the high PDI value of 0.89 is therefore indicative of the polydispersity of the AuNP sample. The average size of the AuNPs was found to be 10.2 nm, which is a suitable size for biosensor applications.

The zeta potential results in table 4.1 are an indicator of the surface charge and stability of the colloidal AuNPs. Zeta potential values exceeding ±30 mV are an indicator of high particle stability with a tendency toward interparticle repulsion, while values lower than ±30 mV indicate a tendency towards aggregation and low particle stability. For AuNPs synthesized using sodium citrate reduction, the surface of the AuNPs is covered with electrostatically attached citrate molecules which confer a highly negative charge and contribute to their stability in solution. The value of -16.43 mV suggests that these AuNPs have been coated with the citrate ions in solution but are not necessarily stable enough to prevent aggregation over time.

Table 4.1 Dynamic light scattering parameters of AuNPs. The measurements are replicates of 3 (n=3).

	1	**2**	**3**	**AVERAGE ± STDDEV**
Size average (nm)	10.31	10.06	10.23	10.20 ± 0.13
Zeta potential (mV)	-14.50	-18.70	-16.10	-16.43 ± 2.12
Polydispersity index	0.89	0.87	0.90	0.89 ± 0.01

4.1.3 Transmission electron microscopy

HRTEM analysis was performed to supplement the UV-Vis and DLS data to provide additional information on the morphology of the AuNPs. Figure 4.3 is a TEM micrograph of the AuNPs at different magnifications. From Figure 4.3a it is observed that the AuNPs vary in size and shape. Although some of the AuNPs are spherical with diameters ranging from 14-18nm, others are rod-shaped (40 nm in length) or amorphous, which indicates a high polydispersity with regard to shape. It was theorized that agglomeration occurred during synthesis when interpreting UV-Vis and DLS data, and Figure 4.3b provides a visual measure of the agglomeration of the sample. The dark sections of the micrograph indicate areas where fewer electrons passed through the sample due to increased thickness of the material, which can be attributed to larger particle diameters of agglomerated particles. Additionally, AuNPs appear to cluster together and overlap instead of being dispersed uniformly throughout the sample.

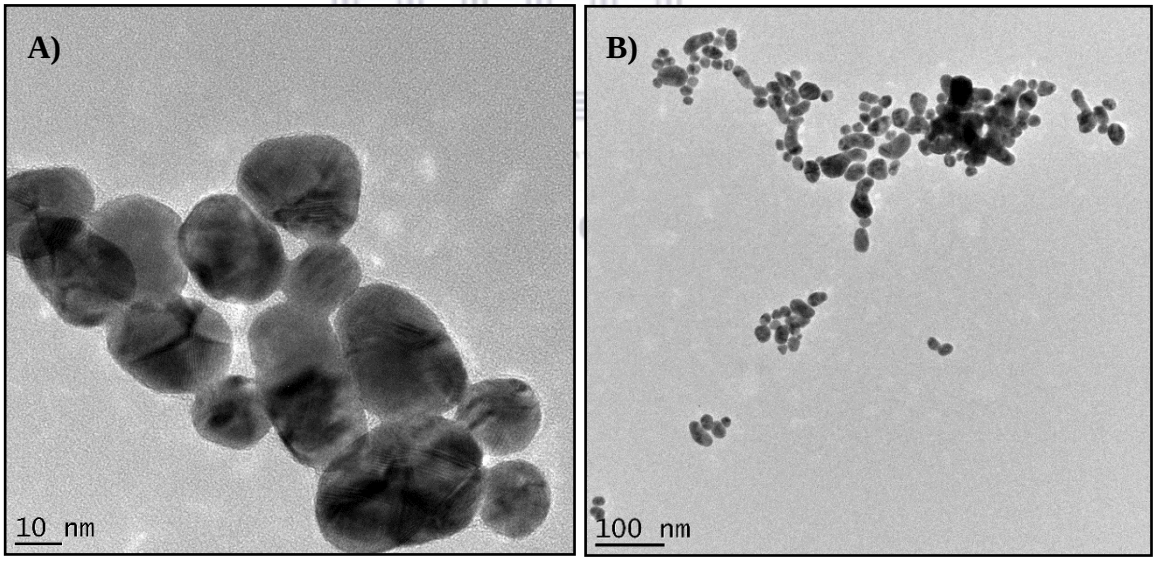

Figure 4.3 TEM micrographs of synthesized AuNPs at a resolution of a) 10nm and b) 100 nm.

4.1.4 Energy-dispersive x-ray spectroscopy

The EDX spectrum in Figure 4.4 provides the elemental composition of the AuNP sample. The spectrum shows the presence of Au, Cu and C characteristic peaks. As the sample was analyzed on a carbon-coated copper grid, the Cu and C peaks are background and can be attributed to the presence of the grid. EDX spectral peaks are unique to the element, and the intensity of the peak is correspondent to the concentration of the element in the sample. The intensity of the Cu peak and lesser intensity of the carbon coating is therefore expected. As the Au is the only other element detectable in the sample this indicates that the AuNP sample is pure and free of chemical contaminants.

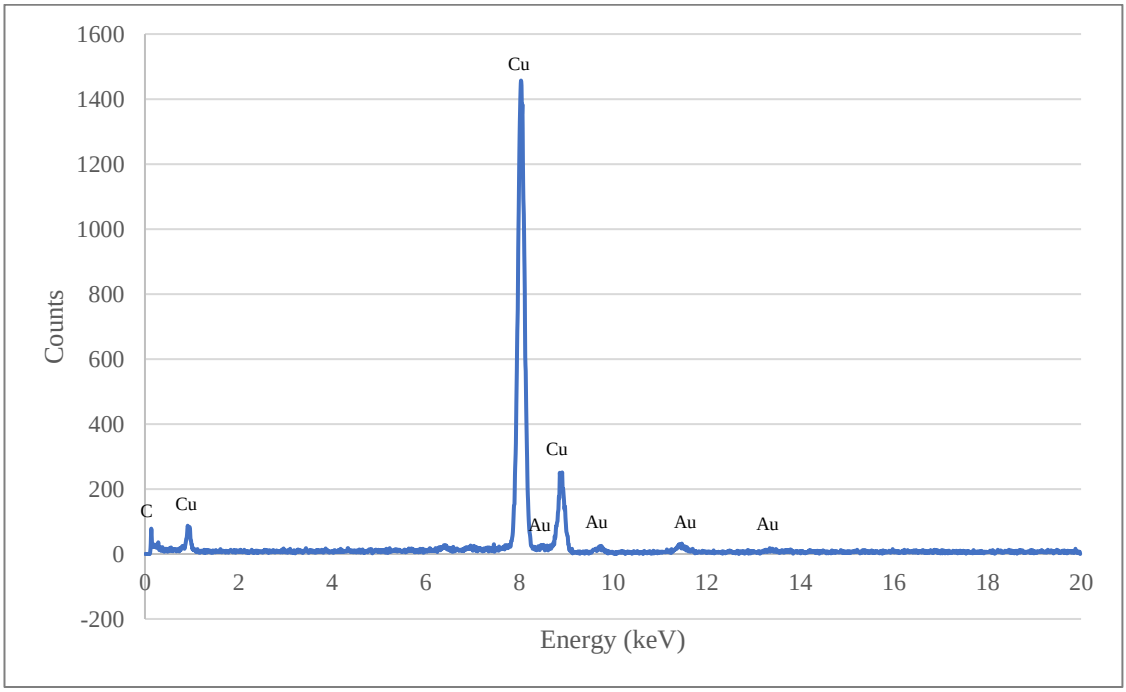

Figure 4.4 EDX spectrum of synthesized AuNPs.

4.1.5 Atomic force microscopy

AFM analysis was used to support the TEM and DLS data to determine the size of the AuNPs and characterize their surface morphology. The topography scan in Figure 4.5 A shows the immobilized AuNPs as light areas of raised height compared to the background of the glass slide. The images were analyzed using ImageJ software and the size range of the AuNPs ranged from 10-200 nm. This is in accordance with the UV-Vis, DLS and TEM data which indicated a majority of smaller AuNPs, but a large degree of polydispersity in the sample with agglomerated AuNPs.

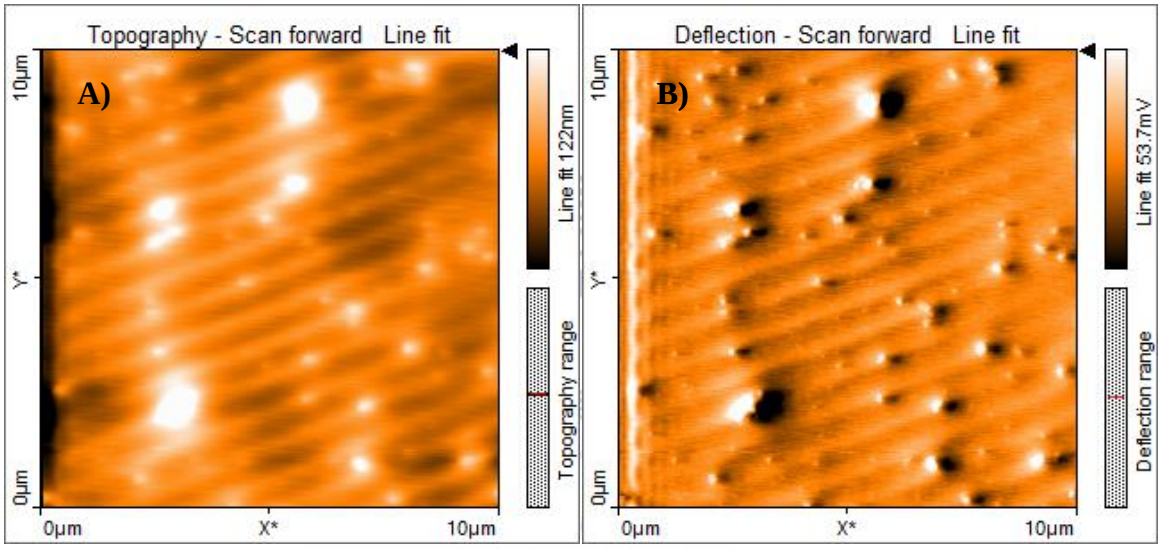

Figure 4.5 AFM images obtained of AuNPs immobilized on a glass slide at a resolution of 5 µm. Image A) shows the topography of the AuNPs and image B) is the error signal image of the same spot.

4.2 Electrochemistry of Immunosensor

4.2.1 Scan rate study

In order to define the electrochemical behaviour of the immunosensor in the absence of the analyte, a CV scan rate study was run at every step of the fabrication process of the GCE. By defining the rate of electron transfer at the working electrode, the effect of the immobilized AuNPs and anti-*Cryptosporidium* antibody (at concentrations of 100, 10 and 1μg.mL^{-1}) on the electrochemistry of the system was determined. A corresponding Randles-Sevcik plot was constructed for each of the modified GCEs according to the Randles-Sevcik equation:

$$i_{pc} = 2.69x10^{8}n^{3/2}AD^{1/2}v^{1/2}C$$

According to this equation, the linear plot of i_o vs. $v^{1/2}$ will yield a linear gradient equal to the diffusion coefficient of the system if the redox process is chemically reversible. The cyclic voltammogram for the bare electrode in ferricyanide in Figure 4.6 is in agreement with reported studies on the electrochemistry of ferricyanide, with one anodic peak and one cathodic peak indicating the oxidation and reduction of the electrolyte. The Randles-Sevcik plots in Figures 4.6-4.10 are all linear and represent reversible redox processes, indicating that modification of the GCE with the AuNPs and differing concentrations of antibodies does not chemically affect the electrolyte in comparison to the bare electrode system.

The diffusion coefficient (D_0) was calculated from the slope of the Randles-Sevcik plot using the Randles-Sevcik equation and is an indication of the rate of electron transport in the system. The geometric surface area of the GCE electrode (0.071 cm^2) was used in all calculations to develop a relative understanding of the effect of modifications. Although the electrolyte is not chemically affected by the modifications and the linearity of the system remains, the effect of the modifications on the diffusion coefficient of the system is apparent in Figures 4.6-4.10 and Table 4.2. The diffusion coefficient derived from the oxidation peak is 5.12 and 5.65 m^{2}s^{-1} for the bare GCE and AuNP-coated GCE respectively. This indicates that the immobilization of AuNPs on the surface of the electrode increases the rate of electron transport. This is expected as AuNPs in biosensors are used to increase the

sensitivity and signal, and the peak signal is enhanced by the AuNPs when directly compared to the bare GCE at a scan rate of 100mV.s^{-1} in Figure 4.11.

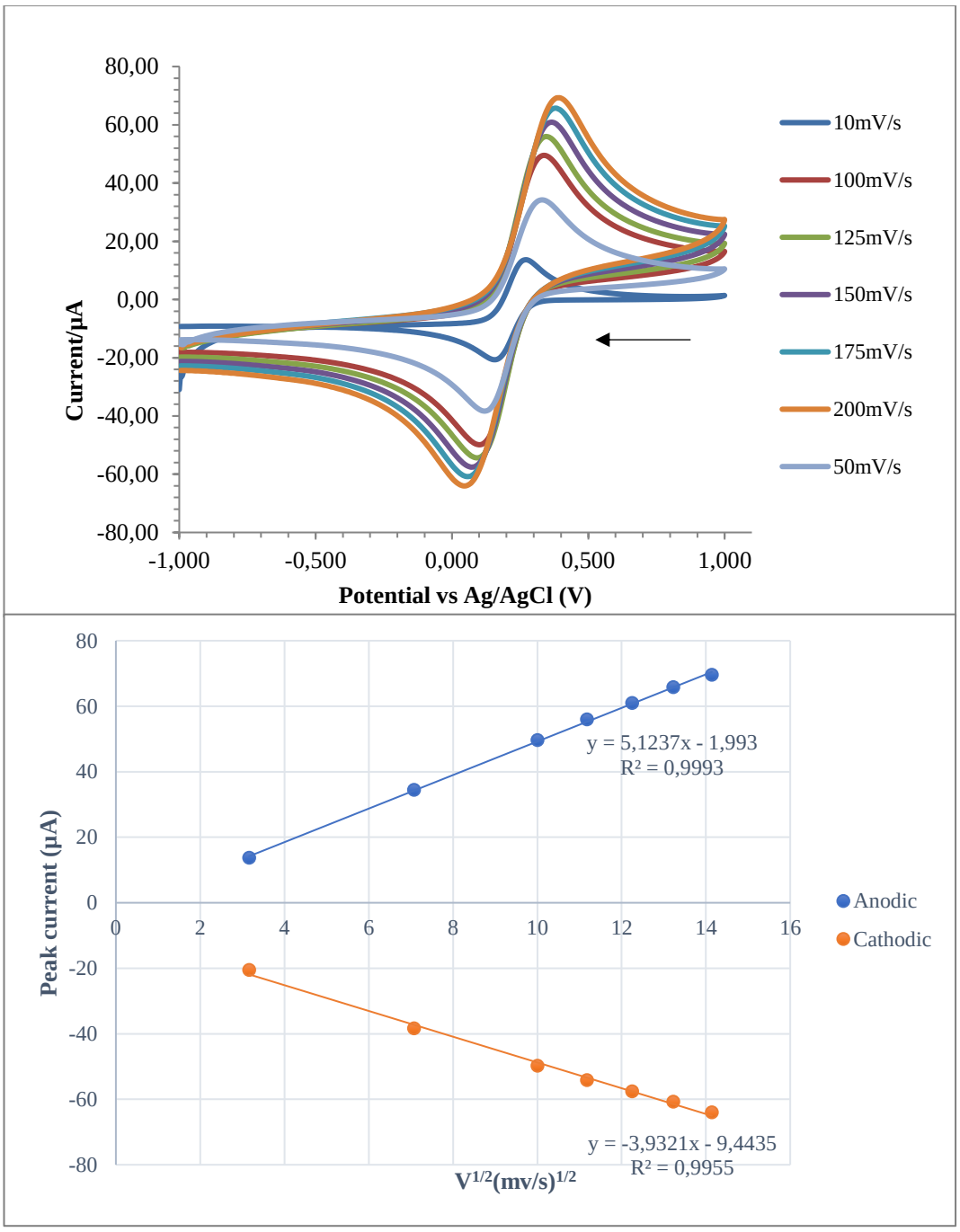

Figure 4.6 Cyclic voltammogram and Randles-Sevcik plot of the ferricyanide/ferrocyanide couple in 0.1M KCl at scan rates ranging from 10-200 mV/s at the bare GCE.

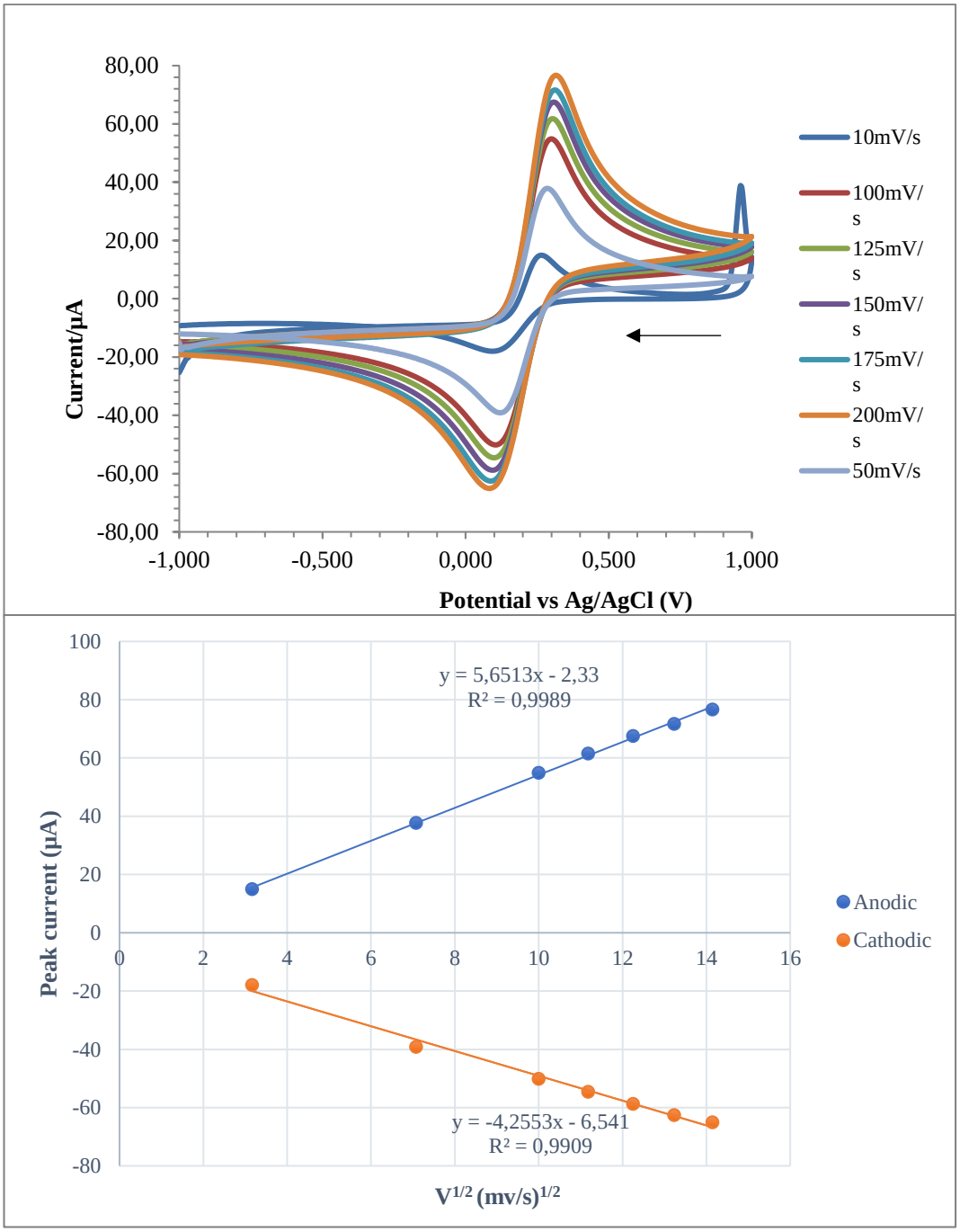

Figure 4.7 Cyclic voltammogram and Randles-Sevcik plot of the ferricyanide/ferrocyanide couple in 0.1M KCl at scan rates ranging from 10-200 mV/s at the AuNP coated GCE.

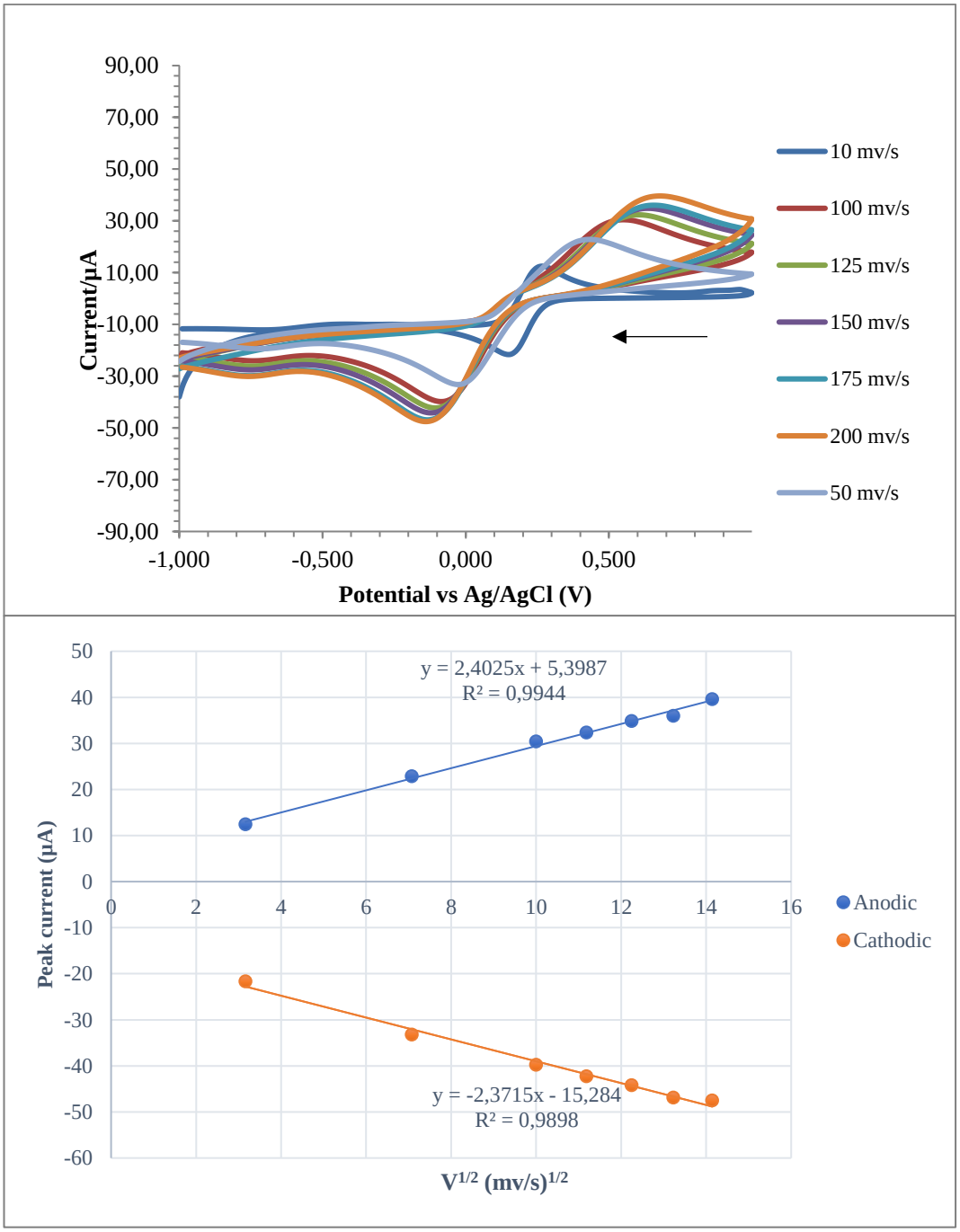

Figure 4.8 Cyclic voltammogram and Randles-Sevcik plot of the ferricyanide/ferrocyanide couple in 0.1M KCl at scan rates ranging from 10-200 mV/s at the AuNP/100 µg.mL^{-1} mAb coated GCE.

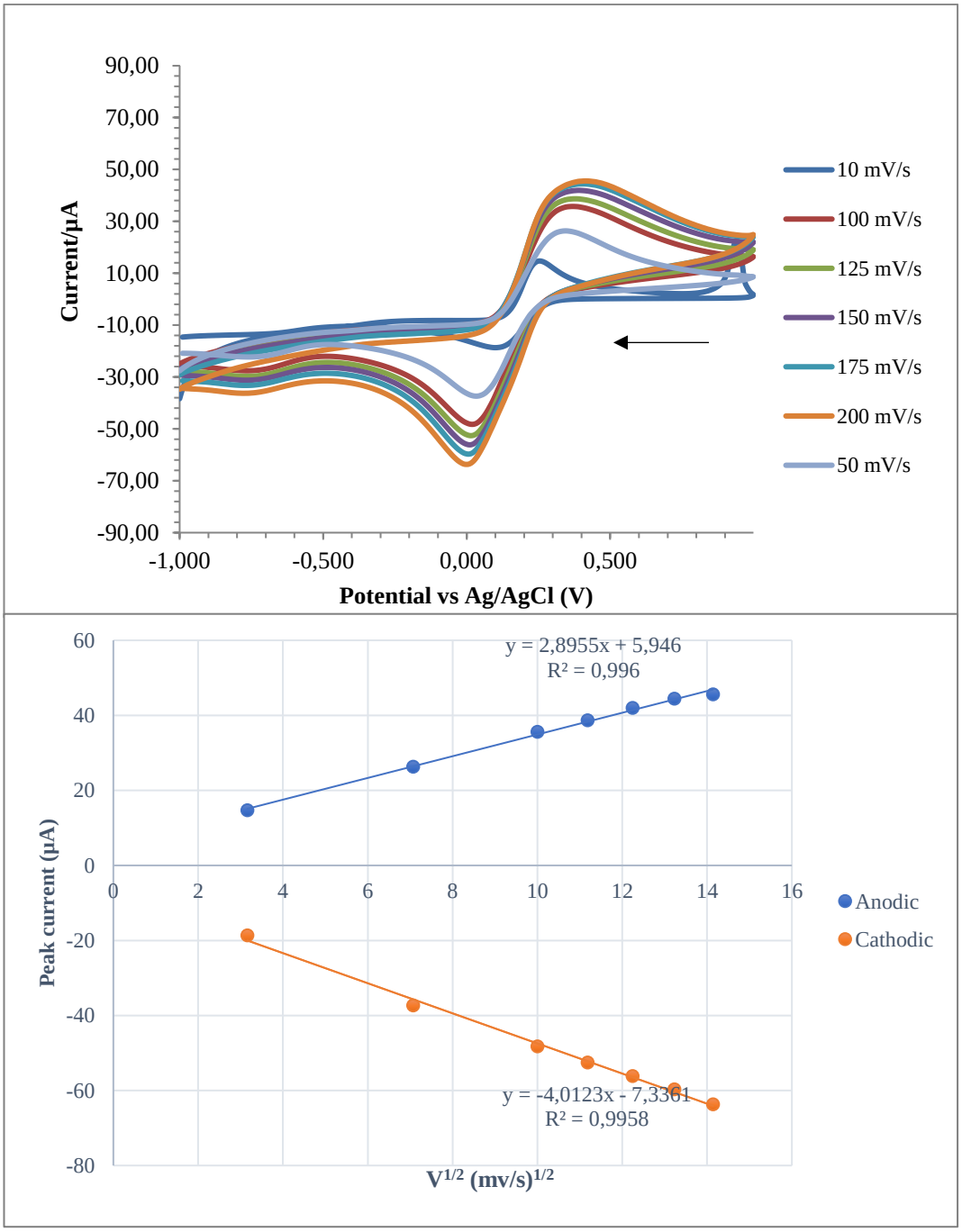

Figure 4.9 Cyclic voltammogram and Randles-Sevcik plot of the ferricyanide/ferrocyanide couple in 0.1M KCl at scan rates ranging from 10-200 mV/s at the AuNP/10 µg.mL^{-1} mAb coated GCE.

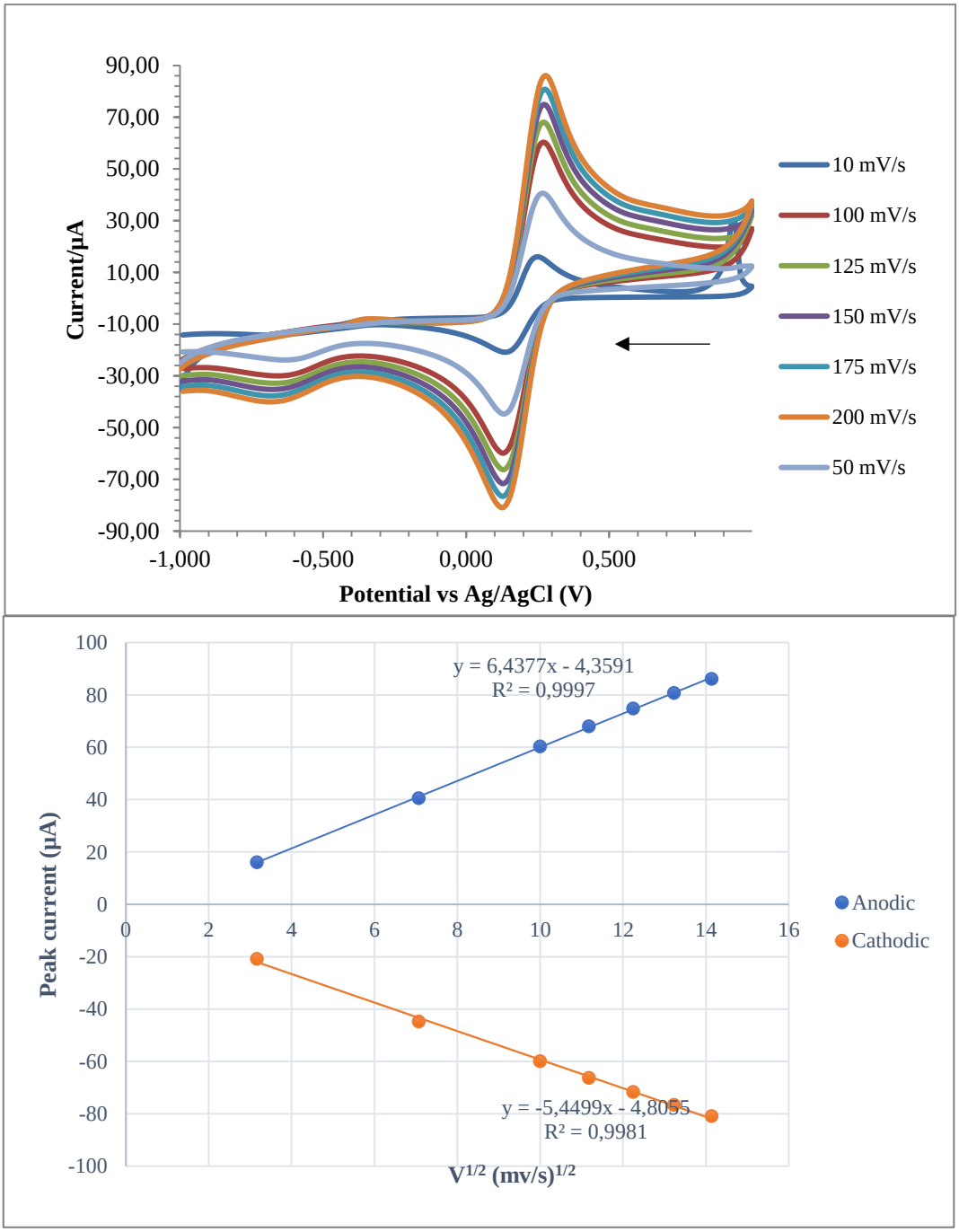

Figure 4.10 Cyclic voltammogram and Randles-Sevcik plot of the ferricyanide/ferrocyanide couple in 0.1M KCl at scan rates ranging from 5-200 mV/s at the rAuNP/1ug.mL^{-1} mAb coated GCE.

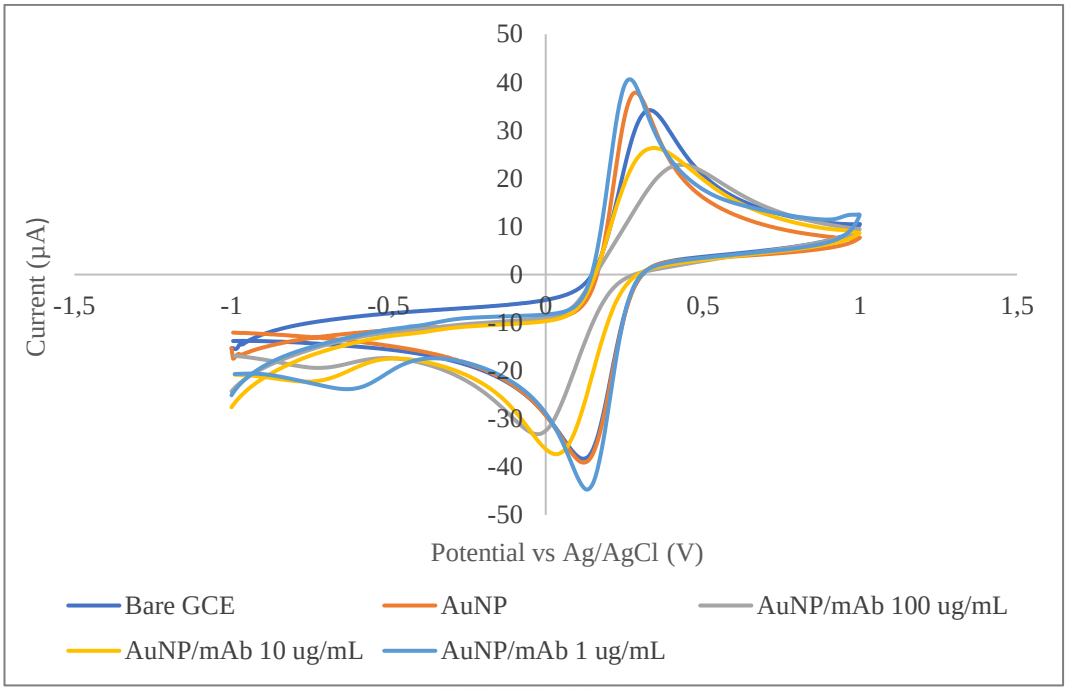

Figure 4.11 Cyclic voltammogram of a) bare GCE electrode in 3mL ferricyanide b) AuNP coated GCE electrode c) AuNP/100ug.mL^{-1} mAb coated GCE d) AuNP/10ug.mL^{-1} mAb coated GCE e) AuNP/1ug.mL^{-1} mAb coated GCE in 3 mL ferricyanide at a scan rate of 100mV/s.

Although the peak current and diffusion coefficient are increased when coating the working electrode with AuNPs, this effect is not very pronounced, with only a 0.2 m^{2}.s^{-1} difference in the diffusion coefficient between the modified and unmodified system (Table 4.3). It is possible that the concentration of AuNPs immobilized on the GCE surface was too low to significantly improve the ferricyanide signal.

The immobilization of the anti-*Cryptosporidium* antibody on the AuNPs appears to impart the largest effect on the system and is the effect is dependent on the concentration of the antibody. The diffusion coefficient for the AuNP/100µg.mL^{-1} modified GCE is decreased from 2.60 m^{2}.s^{-1} in the bare electrode to 1.78 m^{2}s^{-1} and the peak current at 100mV.s^{-1} is seen to nearly half in Figure 4.10. When the concentration of the antibody is decreased in the AuNP/10µg.mL^{-1} modified GCE, the peak current increases slightly and the D^{0} increases to 1.95 m^{2}.s^{-1}. This can be attributed to the thickness of the antibody layer, where the electron diffusion is highest at the lowest antibody concentration (1 µg.mL^{-1}).

Table 4.2 Electrochemical parameters obtained from the characterization of ferrocyanide/ferricyanide redox couple.

Modification	Scan rate (mV/s)	Epa (mV)	Epc (mV)	Ipa (µA)	Ipc (µA)	Eo (mV)	n
	10	269	158	13.74	-20.58	214	0.53
	50	327	120	34.42	-38.40	224	0.29
	100	336	99	49.61	-49.81	218	0.26
	125	345	90	55.93	-54.21	218	0.23
	150	364	71	61.02	-57.60	218	0.20
	175	380	54	65.75	-60.81	217	0.18
Bare	200	389	43	69.54	-64.01	216	0.17
	10	264	111	14.95	-17.89	188	0.39
	50	282	124	37.73	-39.11	203	0.37
	100	298	106	54.93	-50.16	202	0.31
	125	304	99	61.58	-54.57	202	0.29
	150	308	93	67.55	-58.71	201	0.27
	175	312	87	71.74	-62.57	199	0.26
AuNP GCE	200	315	84	76.65	-65.04	200	0.26
	10	259	149	12.42	-21.64	204	0.54
	50	429	-21	22.84	-33.18	204	0.13
	100	539	-91	30.39	-39.79	224	0.09
	125	599	-111	32.34	-42.27	244	0.08
	150	629	-121	34.85	-44.17	254	0.08
	175	669	-131	36.00	-46.86	269	0.07
AuNP/100 µg/mL mAb	200	679	-141	39.62	-47.53	269	0.07
	10	249	99	14.68	-18.68	174	0.39
	50	349	29	26.33	-37.36	189	0.18
	100	389	19	35.63	-48.24	204	0.16
	125	379	19	38.69	-52.56	199	0.16
	150	389	9	41.96	-56.14	199	0.16
	175	409	9	44.44	-59.69	209	0.15
AuNP/10 µg/mL mAb	200	419	1	45.57	-63.68	210	0.14
	10	249	139	16.06	-20.81	194	0.54
	50	269	129	40.61	-44.73	199	0.42
	100	269	129	60.33	-59.86	199	0.42
	125	269	129	68.06	-66.25	199	0.42
	150	269	129	74.85	-71.65	199	0.42
	175	279	129	80.72	-76.56	204	0.39
AuNP/1 µg/mL mAb	200	279	129	86.13	-80.89	204	0.39

Table 4.3 Diffusion coefficient values obtained from the characterization of ferrocyanide/ferricyanide redox couple.

Modification	Peak	Redox Potential	Slope (µA/V.s-1)	D_0 (m^2s^{-1})	R^2
Bare GCE	A	Oxidation	5.12	2.60	1.00
	B	Reduction	3.93	2.27	1.00
AuNP	A	Oxidation	5.65	2.73	1.00
	B	Reduction	4.26	2.37	0.99
AuNP/100 µg/mL mAb	A	Oxidation	2.40	1.78	0.99
	B	Reduction	2.37	1.77	0.99
AuNP/10 µg/mL mAb	A	Oxidation	2.90	1.95	0.99
	B	Reduction	4.01	2.30	0.99
AuNP/1 µg/mL mAb	A	Oxidation	6.44	2.91	0.99
	B	Reduction	5.45	2.68	0.99

4.2.2 Response time optimization

Once the electrochemical behaviour of the immunosensor was determined with scan rate studies, the response time of the immunosensor to the oocysts was determined over a period of 30 minutes to choose an optimal incubation time.

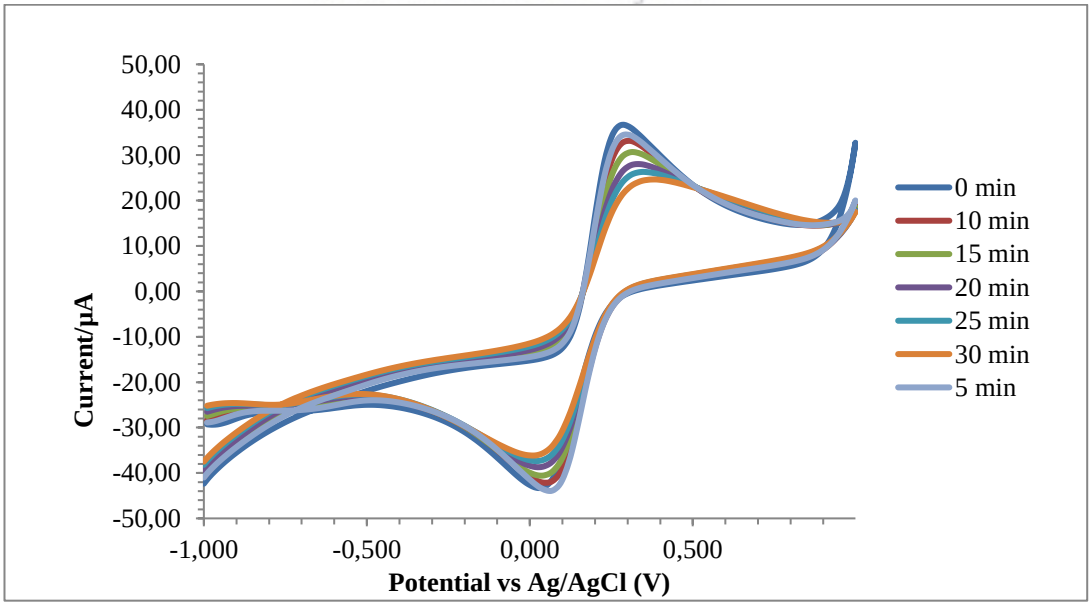

Figure 4.12 Cyclic voltammogram of time-dependent response of immunosensor to addition of 100 oocysts.

Figure 4.12 shows the response of the immunosensor to the addition of 100 oocysts to the system. The response is seen in the reduction of the ferricyanide peak currents for the oxidation and reduction processes. This can be explained by the binding of the oocysts to the surface of the working electrode, inhibiting the electron transfer process and reducing the current. A decrease in the peak current is observed as soon as 5 minutes after addition of the oocysts. The decrease in peak current increases over time, and the decrease in signal is greatest after 30 minutes of incubation (Figure 4.13). Although the 30-minute incubation time gave the highest peak current decrease, a shorter incubation time is preferable for a rapid test and as an observable reduction is seen after 5 minutes, 10 minutes was decided on to optimize the signal strength and minimize the incubation time. Experimentally, concentration curves constructed using a 5-minute incubation time yielded a linear response in comparison to the 10-minute incubation, and a 5-minute incubation period was used for following experiments.

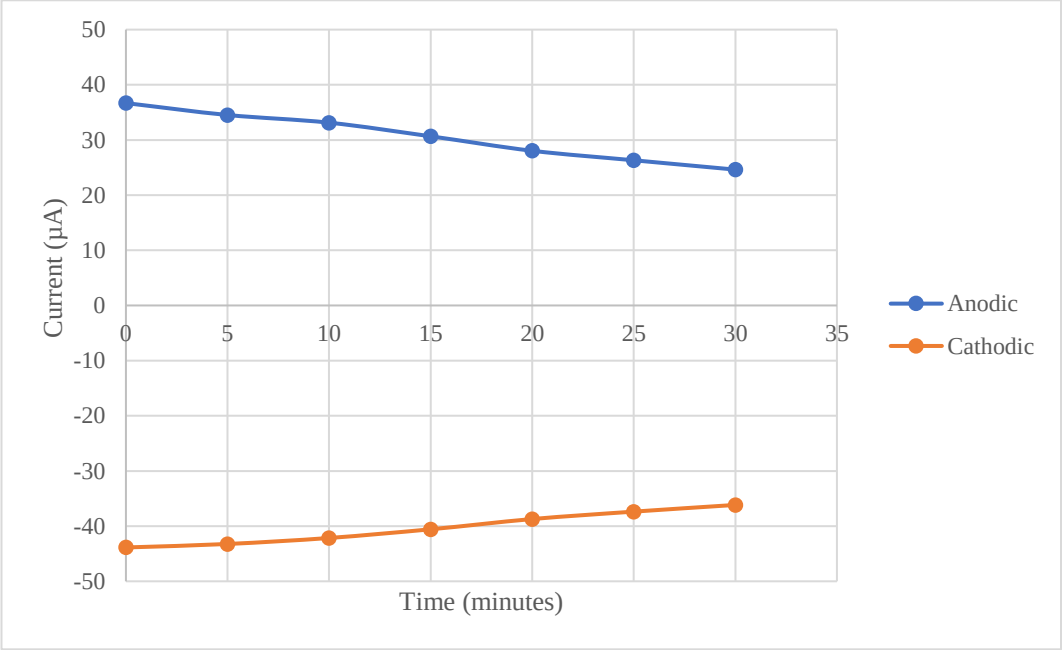

Figure 4.13 Plot of response time vs response current for the addition of 100 oocysts to the immunosensor.

4.2.3 Calibration of concentration response

The concentration response was assessed for different anti-*Cryptosporidium* antibody concentrations to determine the optimal antibody immobilization amount and ensure a strong signal and response to the oocysts. The oocyst concentration was also varied to obtain the optimal detection range of the immunosensor.

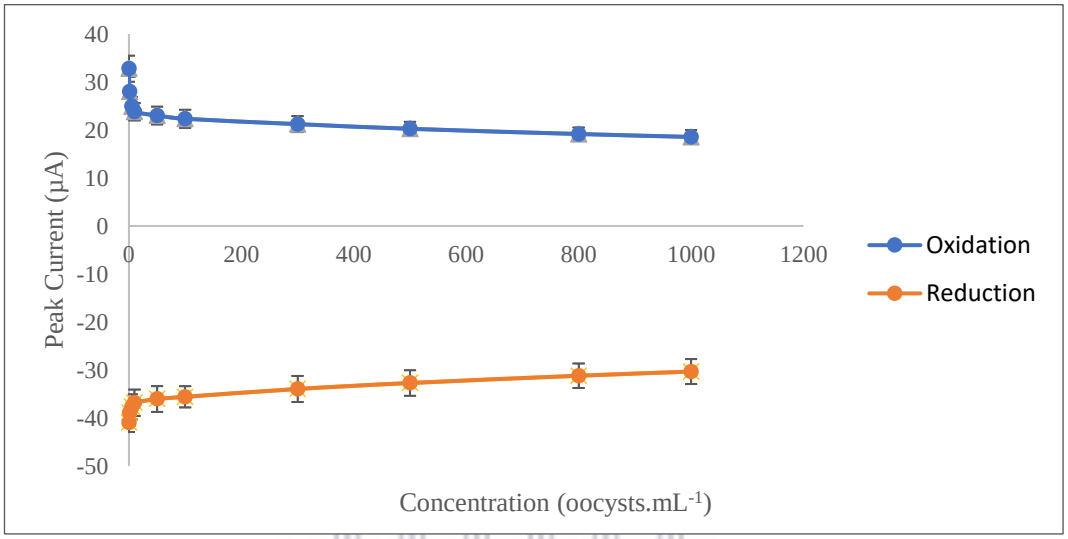

Figure 4.14 Calibration plot of peak current versus the concentration of oocysts (0-1000 oocysts.mL^{-1}) of the immunosensor at a 100 µg.mL^{-1} dilution of antibody in 1 mL ferricyanide. The values represent replicates of three (n=3).

In Figure 4.14, the response of the AuNP/100 µg.mL^{-1} mAb immunosensor to a wide concentration range of 0-1000 oocysts was determined. The response signal appears to be linear from approximately 0-100 oocysts.mL^{-1} but plateaus thereafter and little change in signal is observed after this point. A 20-100 oocyct.mL^{-1} concentration range was therefore further explored in Figure 4.15 and a linear concentration response was found, however, the gradient of the linear slope was low at 0.073 and 0.087 µA/oocyst.mL^{-1} for the oxidation and reduction process respectively.

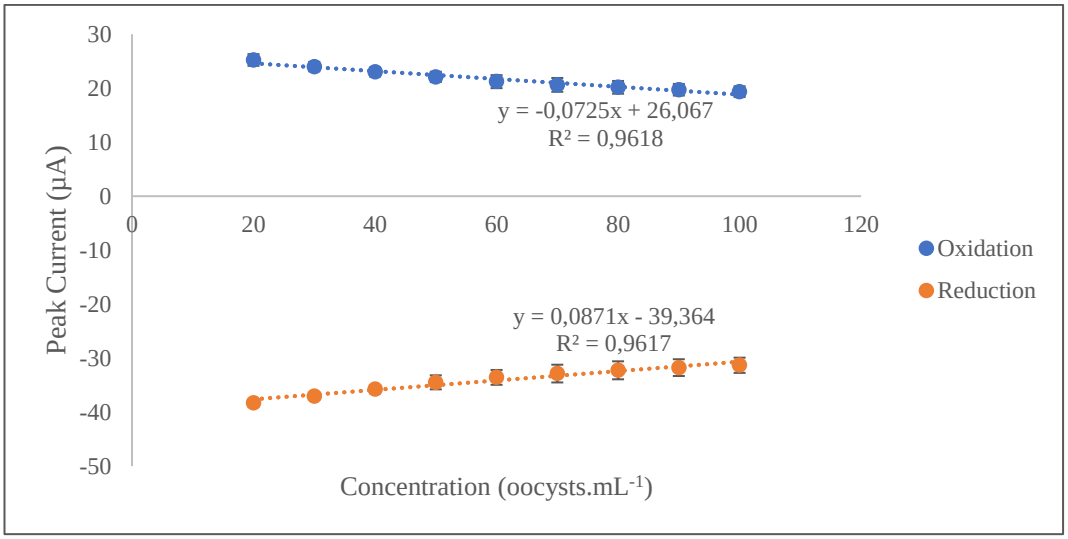

Figure 4.15 Calibration plot of peak current versus the concentration of oocysts (20-100 oocysts.mL^{-1}) of the immunosensor at a 100 µg.mL^{-1} dilution of antibody in 1 mL ferricyanide. The values represent replicates of three (n=3).

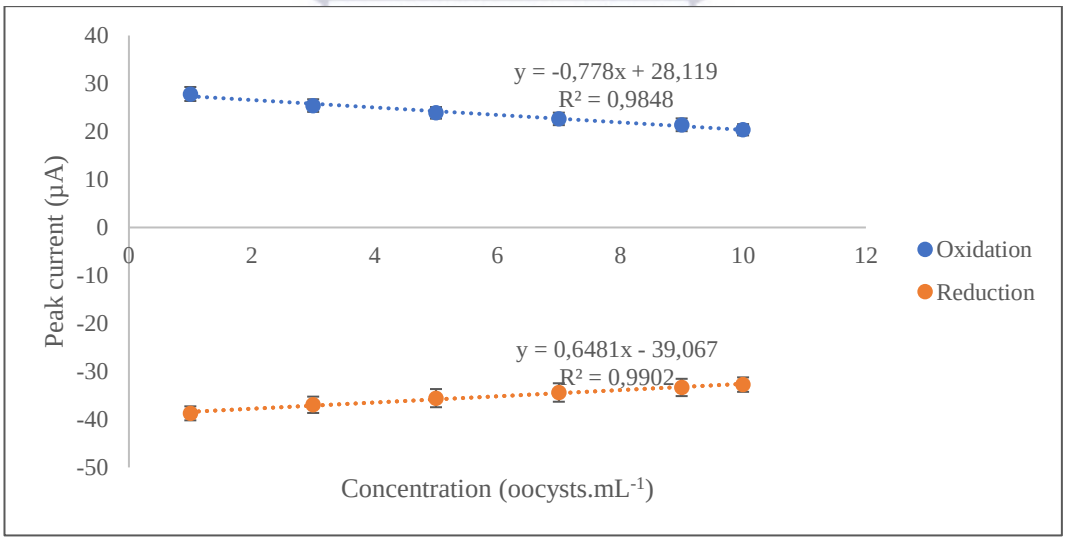

Figure 4.16 Calibration plot of peak current versus the concentration of oocysts (0-10 oocysts.mL^{-1}) of the immunosensor at a 100 µg.mL^{-1} dilution of antibody in 1 mL ferricyanide. The values represent replicates of three (n=3).

In a separate experiment, the response of the immunosensor was further investigated at the same antibody concentration to 0-10 oocysts.mL^{-1} in Figure 4.16. The linear slope of the immunosensor response is the steepest for the lower oocyst concentration, at 0.78 and 0.65 µA/oocyst.mL^{-1} for the oxidation and reduction process. This indicates that the antibodies are quickly saturated by the oocysts in

solution. Although the antibody concentration is very high at 100 µg.mL^{-1} and it is not expected that this should be easily saturated with low amounts of oocyst, it must be noted that the method of immobilizing the antibody on the AuNPs is via physisorption and the orientation of the antibody on the AuNP is random. Therefore, some of the antibody molecules may be bound to the AuNPs at the binding site or be bound to the AuNPs in such a way that the binding site is not easily accessible. This is especially important when considering the relative sizes of the antibody and the analyte. Most antibodies are ~150 kDa or 10 nm in size. As oocysts range between 4.2-5.4 µm in diameter, the binding of one oocyst to an antibody can spatially prevent another oocyst from binding to a correctly orientated antibody. Hence, it may be essential to ensure that all possible antibodies are correctly orientated in future studies to allow the highest possible amount of *Cryptosporidium* oocysts to be bound to the surface of the electrode.

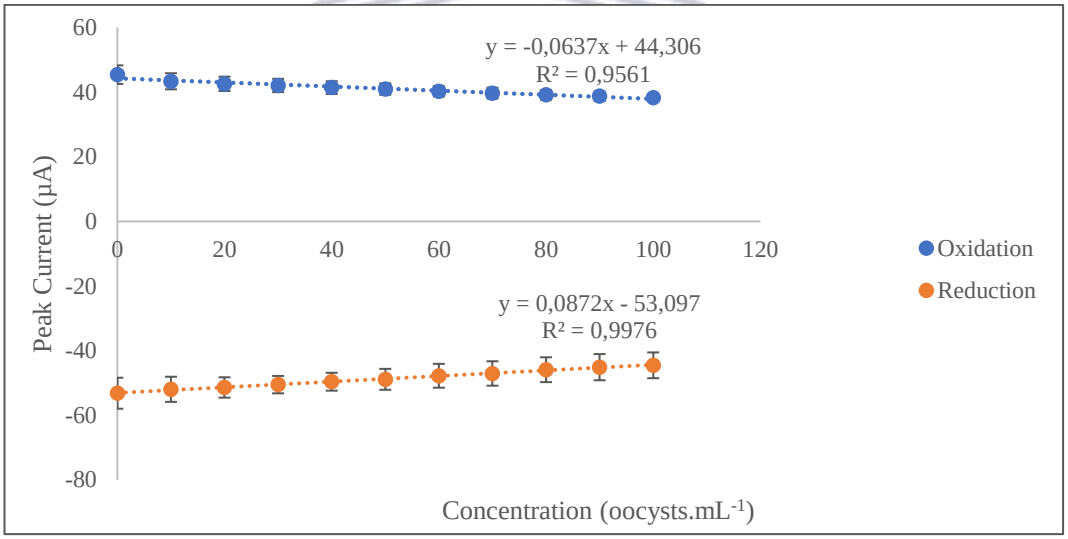

Figure 4.17 Calibration plot of peak current versus the concentration of oocysts (0-100 oocysts.mL^{-1}) of the immunosensor at a 10 µg.mL^{-1} dilution of antibody in 1 mL ferricyanide. The values represent replicates of three (n=3).

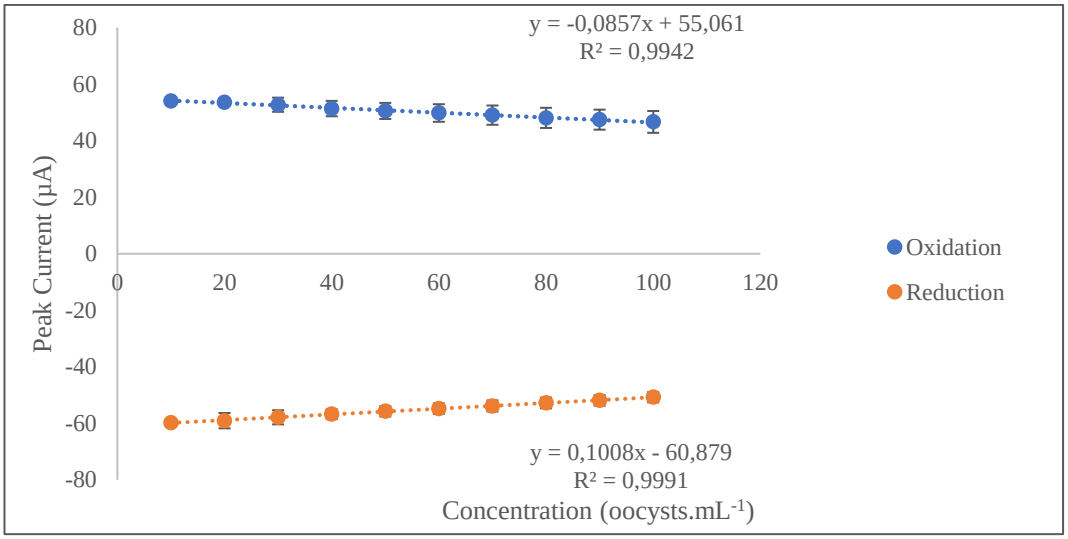

Figure 4.18 Calibration plot of peak current versus the concentration of oocysts (0-100 oocysts.mL^{-1}) of the immunosensor at a 1 µg.mL^{-1} dilution of antibody in 1 mL ferricyanide. The values represent replicates of three (n=3).

The low oocyst concentration saturation effect is also seen in Figures 4.17 and 4.18, which show the response of the immunosensor from 0-100 oocysts.mL^{-1} for antibody concentrations of 10 and 1 µg.mL^{-1} respectively. Both antibody concentrations show similar rates of peak current change, even though the peak currents are higher in comparison to Figures 4.13-15 due to the lower amount of antibody immobilized on the surface.

Table 4.4 Calibration and statistical parameters for performance of immunosensor.

	Anodic			**Cathodic**		
	100 µg/mL	10 µg/mL	1 µg/mL	100 µg/mL	10 µg/mL	1 µg/mL
AVE LOD±STDDEV (oocysts/mL)	7.32± 0.39	123.66± 48.21	50.89± 15.86	6.09± 0.23	105.89± 50.66	37.00± 3.76
AVE LOQ±STDDEV (oocysts/mL)	22.19± 1.17	374.73± 146.10	154.21± 48.07	18.47± 0.71	320.87± 153.52	112.12± 11.39
R^2	0.98	0.96	0.99	0.99	1.00	1.00
AVESLOPE±STDDEV	0.78± 0.04	0.06± 0.02	0.09± 0.03	0.65± 0.04	0.09± 0.03	0.10± 0.01
SD of Blank	1.73	2.39	1.32	1.20	2.80	1.13

The performance of the immunosensor at differing concentrations of immobilized anti-*Cryptosporidium* mAb was assessed using the limit of detection (LOD) and limit of quantification (LOQ) parameters. The LOD represents the lowest concentration that can be observed with a sufficient degree of confidence or statistical significance, while the LOQ is the lowest signal that can be observed to determine the concentration of an analyte with accuracy. These equations are defined by:

$$LOD = \frac{3.3 \times SD}{b}$$

$$LOQ = \frac{10 \times SD}{b}$$

Where:

SD = standard deviation of blank

b = slope of the regression line

In Table 4.4 it can be seen that the immunosensor design that yielded the lowest LOD and LOQ values with low values of standard error was the design with the highest concentration of anti-*Cryptosporidium* mAb (100 $\mu g.mL^{-1}$). Although all of the mAb concentrations produced plots with a high degree of linearity, the slopes or rate of response of the 10 and 1 $\mu g.mL^{-1}$ mAb immunosensor were too low to detect the *Cryptosporidium* oocysts at low concentrations with any statistical significance.

Additionally, the LOD/LOQ standard deviation of the 10 and 1 $\mu g.mL^{-1}$ mAb immunosensors indicates that the response was not reproducible, with a high margin of error in the analysis. As previously discussed, the low concentration of mAb that is accessible for binding to the oocysts results in an early saturation of the mAb and low signal responses even at low oocyst concentrations. This indicates that if a physisorption method of immobilization of mAb onto the AuNPs is used, it is important to use high mAb concentrations to obtain the best response from the sensor.

4.3 *Cryptosporidium* staining

As the stock solution of *Cryptosporidium* was at a concentration of $1.25x10^6$ oocysts.mL^{-1}, a working stock (1000 oocysts.mL^{-1}) had to be prepared for immunosensor characterization with a series of serial dilutions. In order to confirm that oocysts were present in the working stock used for testing the immunosensor, the oocyst working stock was validated by staining the oocysts with a modified Ziehl-Neelsen method and by examining the oocysts with light microscopy. In this technique, carbol fuchsin stains the oocysts red and background microorganisms blue. In Figure 4.19, it can be seen that several singular oocysts were stained red and could be identified, confirming the presence of oocysts in the working stock solution. As this is a qualitative method, the exact concentration of oocysts in the working stock could not be confirmed, and a future consideration could be to use fluorescent labels and flow cytometry to validate the exact number of oocysts. It is therefore recommended that the detection limit values of the immunosensor be interpreted with this in mind.

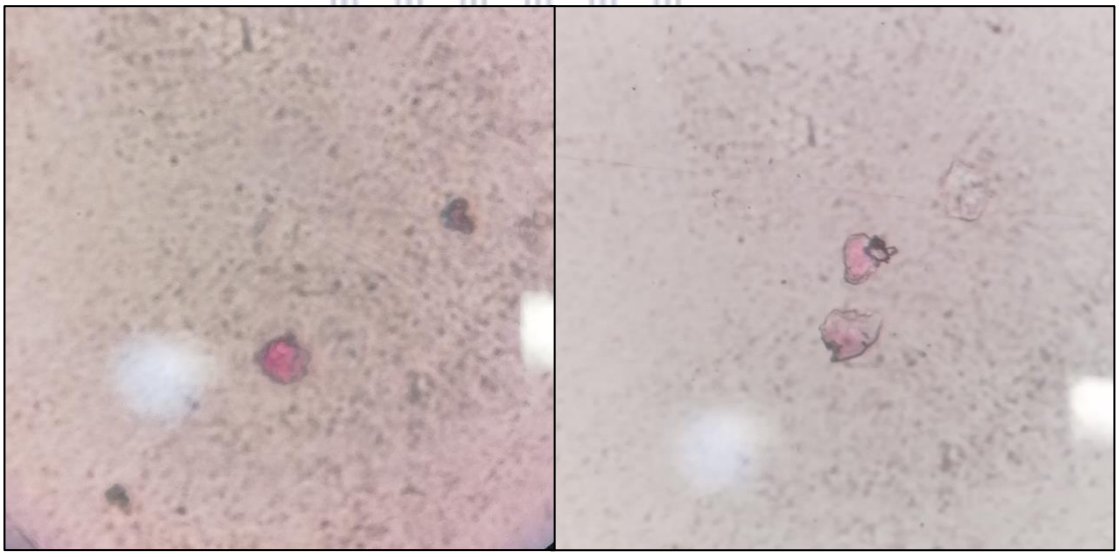

Figure 4.19: Image of carbol fuchsin stained oocysts (red) from working stock dilution of *Cryptosporidium* under 400x magnification.

5. Chapter 5: Conclusion and future perspectives

This chapter summarizes the key results of the immunosensor and contrasts the performance of the immunosensor to the gold standard of *Cryptosporidium* detection, USEPA Method 1623. The limitations of the design and study are discussed, and recommendations are given for consideration in future work.

In recent years, a shift in research focus has occurred from using conventional techniques to the development of biosensors for *Cryptosporidium* monitoring. Despite achieving low detection limits, many of the sensors developed for *Cryptosporidium* are limited due to the complexity of their design. Several electrochemical biosensors developed for *Cryptosporidium* detection require multiple labelling steps for their fabrication, the use of both a primary and secondary antibody, expensive labels, and extraction of mRNA prior to the detection step. Other biosensor protocols utilize detection methods such as SERRS and SPR which require expensive instrumentation and trained personnel, limiting their accessibility.

The purpose of this study was therefore to fabricate a simple immunosensor design for detection of *Cryptosporidium*. The immunosensor designed was a label-free system, using immobilization of oocysts at the surface of the working electrode via mAb binding to hinder electron transfer and decrease the signal of the electrolyte, ferricyanide. The simplicity of the design resulted in an easily fabricated, low-cost immunosensor, however, it can be argued that it was oversimplified. The immobilization strategy used for depositing the mAb onto the electrode surface was physisorption and as this is a physical binding technique, there was no control over the orientation of the antibody. Additionally, the loading of the AuNPs was not standardized as the AuNPs used were not uniform in shape and size, parameters that could be controlled in future studies by controlling the pH of the synthesis reaction.

Despite the design flaws, the immunosensor was able to detect *Cryptosporidium* at detection limits comparable to conventional techniques. The lowest calibration

standard for the USEPA Method 1623 is between 40-500 oocysts.10 L^{-1} (accounting for the concentration of the bulk volume of the sample during processing), while the immunosensor yielded a detection limit of 7.32 and 6.09 oocysts.mL^{-1} for the oxidation and reduction processes, respectively. As few as 10 oocysts ingested can cause disease in healthy individuals, and low limits of detection are imperative for water monitoring of *Cryptosporidium*. The immunosensor fabricated in this study is therefore a good candidate for a low-detection capability alternative to the USEPA Method 1623. If the immunosensor is optimized for sensitive, on-site analysis, this will prevent the need for the processing of 10L of water by Method 1623, as the large volumes required for processing are primarily needed to account for the low sensitivity of the method. This will reduce the labour intensity and processing times needed for *Cryptosporidium* detection in water.

Future studies must be completed to determine the suitability of the sensor for application of samples collected on-site to the system. Ideally, the system should function to detect oocysts in minimally processed environmental samples, however, this study has only evaluated the detection of purified oocysts in a PBS buffer. If interferences from environmental water matrices impact the selectivity and sensitivity of the sensor, sample preparation will have to include filtration of the water sample to remove debris. If it is necessary to process the samples by filtration to remove debris, it will be essential to include oocyst recovery studies to determine the number of oocysts lost in the filtration step. This would involve spiking various water matrices with a known concentration of oocysts and determining the recovery rate by enumeration of the oocysts with both the immunosensor and a conventional detection method.

The main limitation of this study is hence the lack of testing of the immunosensor in real water matrices such as drinking water, ground water and surface water. Ideally, several water samples would be spiked with a known concentration of *Cryptosporidium* oocysts and tested to determine the matrix effects on the system. There is a large amount of debris in unprocessed surface waters as well as microbiological contaminants that may interfere with the specificity and selectivity of the immunosensor. The pH of the real water sample will also likely not be at pH

7.2, unlike the buffered oocyst test solution used in this study, and this may affect the current response and the stability of both the AuNPs and the mAb. Treated drinking water may also contain chemicals that chemically interact with the electrolyte, altering the electrochemical signal. Not including a study to examine matrix effects therefore limits this work to a proof of concept as the experiments were strictly controlled, and oocysts were prepared in a PBS standard only. This is especially important considering that the immunosensor is a label-free system and the specificity of the system may be lower, as any contaminant that decreases the ferricyanide peak current signal may be mistaken for *Cryptosporidium*. A possible solution to this is the application of the sample directly to the modified GCE or, alternatively, a screen-printed carbon electrode, and not to the electrolyte solution.

Due to the lack of control over antibody orientation, a high level of mAb is needed (100 $\mu g.mL^{-1}$) to achieve reproducible, low-level detection of oocysts. The immunosensor is relatively low cost as it is a label-less system, with a once-off cost of the electrodes. However, when high concentrations of mAb are used the cost is increased substantially. Future research should therefore focus on optimizing the antibody immobilization process with a targeted anchoring strategy to not only reduce the cost of the immunosensor, but also to improve the detection limit.

Another important consideration for improving the sensitivity of the immunosensor is the detection principle itself. Instead of monitoring the change in current of the ferricyanide redox reaction with cyclic voltammetry, a capacitance probing method could be used either with or without a redox probe. Electrochemical impedance spectroscopy is a technique that measures the impedance in a circuit, allowing for analysis of biorecognition events such as antibody-antigen recognition or whole-cell capture [96]. This technique has been used for aptameric recognition of analytes in the presence and absence of ferricyanide as a redox mediator [97], [98]. The affinity binding event between the mAb and the oocyst would be captured as a concentration-dependent capacitance change by EIS, offering highly sensitive detection that is a promising strategy that could be used in future studies.

References

[1] F. A. Nime, J. D. Burek, D. L. Page, M. A. Holscher, and J. H. Yardley, "Acute enterocolitis in a human being infected with the protozoan Cryptosporidium.," *Gastroenterology*, vol. 70, no. 4, pp. 592–598, Apr. 1976.

[2] G. J. Leitch and Q. He, "Cryptosporidiosis-an overview.," *J. Biomed. Res.*, vol. 25, no. 1, pp. 1–16, Jan. 2012, doi: 10.1016/S1674-8301(11)60001-8.

[3] D. B. Huang and A. C. White, "An Updated Review on Cryptosporidium and Giardia," *Gastroenterol. Clin. North Am.*, vol. 35, no. 2, pp. 291–314, 2006, doi: 10.1016/j.gtc.2006.03.006.

[4] W. Checkley *et al.*, "A review of the global burden, novel diagnostics, therapeutics, and vaccine targets for cryptosporidium," *Lancet Infect. Dis.*, vol. 15, no. 1, pp. 85–94, 2015, doi: 10.1016/S1473-3099(14)70772-8.

[5] K. L. Kotloff *et al.*, "Burden and aetiology of diarrhoeal disease in infants and young children in developing countries (the Global Enteric Multicenter Study, GEMS): a prospective, case-control study.," *Lancet (London, England)*, vol. 382, no. 9888, pp. 209–222, Jul. 2013, doi: 10.1016/S0140-6736(13)60844-2.

[6] S. Gunasekera *et al.*, "Organoids and bioengineered intestinal models: Potential solutions to the Cryptosporidium culturing dilemma," *Microorganisms*, vol. 8, no. 5, 2020, doi: 10.3390/microorganisms8050715.

[7] P. C. Okhuysen, C. L. Chappell, J. H. Crabb, C. R. Sterling, and H. L. DuPont, "Virulence of three distinct Cryptosporidium parvum isolates for healthy adults.," *J. Infect. Dis.*, vol. 180, no. 4, pp. 1275–1281, Oct. 1999, doi: 10.1086/315033.

[8] I. Campbell, A. S. Tzipori, G. Hutchison, and K. W. Angus, "Effect of disinfectants on survival of cryptosporidium oocysts.," *Vet. Rec.*, vol. 111, no. 18, pp. 414–415, Oct. 1982, doi: 10.1136/vr.111.18.414.

[9] H. V SMITH, "Cryptosporidium and water: a review," *Water Environ. J.*, vol. 6, no. 4, pp. 443–451, 1992.

[10] R. M. Genta, C. L. Chappell, A. C. White Jr, K. T. Kimball, and R. W. Goodgame, "Duodenal morphology and intensity of infection in AIDS-related intestinal cryptosporidiosis," *Gastroenterology*, vol. 105, no. 6, pp. 1769–1775, 1993.

[11] W. Checkley, L. D. Epstein, R. H. Gilman, R. E. Black, L. Cabrera, and C. R. Sterling, "Effects of Cryptosporidium parvum infection in Peruvian children: growth faltering and subsequent catch-up growth.," *Am. J. Epidemiol.*, vol. 148, no. 5, pp. 497–506, Sep. 1998, doi: 10.1093/oxfordjournals.aje.a009675.

[12] D. F. McCole, L. Eckmann, F. Laurent, and M. F. Kagnoff, "Intestinal

epithelial cell apoptosis following Cryptosporidium parvum infection.," *Infect. Immun.*, vol. 68, no. 3, pp. 1710–1713, Mar. 2000, doi: 10.1128/IAI.68.3.1710-1713.2000.

[13] F. E. Adeyemo, G. Singh, P. Reddy, and T. A. Stenström, "Methods for the detection of Cryptosporidium and Giardia: From microscopy to nucleic acid based tools in clinical and environmental regimes," *Acta Trop.*, vol. 184, no. April 2017, pp. 15–28, 2018, doi: 10.1016/j.actatropica.2018.01.011.

[14] A. R. Jex, H. V. Smith, P. T. Monis, B. E. Campbell, and R. B. Gasser, "Cryptosporidium - Biotechnological advances in the detection, diagnosis and analysis of genetic variation," *Biotechnol. Adv.*, vol. 26, no. 4, pp. 304–317, 2008, doi: 10.1016/j.biotechadv.2008.02.003.

[15] U. Ghoshal, V. Jain, A. Dey, and P. Ranjan, "Evaluation of enzyme linked immunosorbent assay for stool antigen detection for the diagnosis of cryptosporidiosis among HIV negative immunocompromised patients in a tertiary care hospital of northern India," *J. Infect. Public Health*, vol. 11, no. 1, pp. 115–119, 2018, doi: https://doi.org/10.1016/j.jiph.2017.06.007.

[16] N. A. Foudraine *et al.*, "Improvement of chronic diarrhoea in patients with advanced HIV-1 infection during potent antiretroviral therapy.," *AIDS*, vol. 12, no. 1, pp. 35–41, Jan. 1998, doi: 10.1097/00002030-199801000-00005.

[17] R. Mele, M. A. Gomez Morales, F. Tosini, and E. Pozio, "Indinavir reduces Cryptosporidium parvum infection in both in vitro and in vivo models.," *Int. J. Parasitol.*, vol. 33, no. 7, pp. 757–764, Jul. 2003, doi: 10.1016/s0020-7519(03)00093-6.

[18] J. F. Rossignol, A. Ayoub, and M. S. Ayers, "Treatment of diarrhea caused by Cryptosporidium parvum: a prospective randomized, double-blind, placebo-controlled study of Nitazoxanide.," *J. Infect. Dis.*, vol. 184, no. 1, pp. 103–106, Jul. 2001, doi: 10.1086/321008.

[19] J.-F. Rossignol, S. M. Kabil, Y. el-Gohary, and A. M. Younis, "Effect of nitazoxanide in diarrhea and enteritis caused by Cryptosporidium species.," *Clin. Gastroenterol. Hepatol. Off. Clin. Pract. J. Am. Gastroenterol. Assoc.*, vol. 4, no. 3, pp. 320–324, Mar. 2006, doi: 10.1016/j.cgh.2005.12.020.

[20] B. Amadi *et al.*, "Effect of nitazoxanide on morbidity and mortality in Zambian children with cryptosporidiosis: a randomised controlled trial.," *Lancet (London, England)*, vol. 360, no. 9343, pp. 1375–1380, Nov. 2002, doi: 10.1016/S0140-6736(02)11401-2.

[21] J. F. Rossignol *et al.*, "A double-'blind' placebo-controlled study of nitazoxanide in the treatment of cryptosporidial diarrhoea in AIDS patients in Mexico.," *Trans. R. Soc. Trop. Med. Hyg.*, vol. 92, no. 6, pp. 663–666, 1998, doi: 10.1016/s0035-9203(98)90804-5.

[22] W. R. Mac Kenzie *et al.*, "A massive outbreak in Milwaukee of cryptosporidium infection transmitted through the public water supply.," *N. Engl. J. Med.*, vol. 331, no. 3, pp. 161–167, Jul. 1994, doi: 10.1056/NEJM199407213310304.

[23] P. R. Hunter, R. M. Chalmers, Q. Syed, L. S. Hughes, S. Woodhouse, and L. Swift, "Foot and mouth disease and cryptosporidiosis: possible interaction between two emerging infectious diseases.," *Emerg. Infect. Dis.*, vol. 9, no. 1, pp. 109–112, Jan. 2003, doi: 10.3201/eid0901.020265.

[24] S. Dong *et al.*, "Prevalence of Cryptosporidium Infection in the Global Population: A Systematic Review and Meta-analysis," *Acta Parasitol.*, vol. 65, no. 4, pp. 882–889, 2020, doi: 10.2478/s11686-020-00230-1.

[25] E. Scallan *et al.*, "Foodborne illness acquired in the United States--major pathogens.," *Emerg. Infect. Dis.*, vol. 17, no. 1, pp. 7–15, Jan. 2011, doi: 10.3201/eid1701.p11101.

[26] S. A. Squire and U. Ryan, "Cryptosporidium and Giardia in Africa: current and future challenges," *Parasites and Vectors*, vol. 10, no. 1, pp. 1–32, 2017, doi: 10.1186/s13071-017-2111-y.

[27] L. A. Bartelt *et al.*, "High anti-cryptosporidium parvum igg seroprevalence in hiv-infected adults in limpopo, south africa," *Am. J. Trop. Med. Hyg.*, vol. 89, no. 3, pp. 531–534, 2013, doi: 10.4269/ajtmh.12-0550.

[28] B. Omoruyi, F. Matongo, N. T. Nkwetshana, E. Green, A. M. Clarke, and R. N. Ndip, "Environmental and demographic risk factors associated with the prevalence of Cryptosporidium infection in the Alice rural settlements of the Eastern Cape Province of South Africa: A pilot study," *Rev. Environ. Health*, vol. 26, no. 2, pp. 127–133, 2011, doi: 10.1515/REVEH.2011.017.

[29] D. Moodley, T. Jackson, V. Gathiram, and J. Van Den Ende, "Cryptosporidium infections in children in Durban Seasonal variation, age distribution and disease status," *South African Med. J.*, vol. 79, no. 3, pp. 296–297, 1991.

[30] B. A. Leav *et al.*, "Analysis of sequence diversity at the highly polymorphic Cpgp40/15 locus among Cryptosporidium isolates from human immunodeficiency virus-infected children in South Africa," *Infect. Immun.*, vol. 70, no. 7, pp. 3881–3890, 2002, doi: 10.1128/IAI.70.7.3881-3890.2002.

[31] B. Haldewang, "The state of water in South Africa – are we heading for a crisis?," *Inst. Futur. Res.*, vol. 7, no. 01, pp. 1–5, 2009.

[32] R. Kfir, C. Hilner, M. du Preez, and B. Bateman, "Studies on the prevalence of Giardia cysts and Cryptosporidium oocysts in south African water," *Water Sci. Technol.*, vol. 31, no. 5–6, pp. 435–438, 1995, doi: 10.1016/0273-1223(95)00307-9.

[33] M. Dungeni and M. N. B. Momba, "The abundance of cryptosporidium and giardia spp. in treated effluents produced by four wastewater treatment

plants in the gauteng province of South africa," *Water SA*, vol. 36, no. 4, pp. 425–432, 2010, doi: 10.4314/wsa.v36i4.58413.

[34] A. M. Nasser, "Removal of Cryptosporidium by wastewater treatment processes: A review," *J. Water Health*, vol. 14, no. 1, pp. 1–13, 2016, doi: 10.2166/wh.2015.131.

[35] S. S. Division, "SANS 241-1 : 2011 SOUTH AFRICAN NATIONAL STANDARD Drinking water Part 1 : Microbiological , physical , aesthetic," 2011.

[36] Usepa, "Method 1623:," *Control*, no. December, 2005.

[37] P. Pavli, S. Venkateswaran, M. Bradley, and H. Bridle, "Enhancing Cryptosporidium parvum recovery rates for improved water monitoring," *Chemosphere*, vol. 143, pp. 57–63, 2016, doi: https://doi.org/10.1016/j.chemosphere.2015.05.021.

[38] H. V. Smith and R. A. B. Nichols, "Cryptosporidium: Detection in water and food," *Exp. Parasitol.*, vol. 124, no. 1, pp. 61–79, 2010, doi: 10.1016/j.exppara.2009.05.014.

[39] T. Wohlsen and M. Katouli, "A review of the existing methods for detection, enumeration and inactivation of Cryptosporidium in surface waters," *J. Water Supply Res. Technol. - AQUA*, vol. 57, no. 2, pp. 65–77, 2008, doi: 10.2166/aqua.2008.030.

[40] A. Efstratiou, J. Ongerth, and P. Karanis, "Evolution of monitoring for Giardia and Cryptosporidium in water," *Water Res.*, vol. 123, pp. 96–112, 2017, doi: 10.1016/j.watres.2017.06.042.

[41] A. Fall, R. C. A. Thompson, R. P. Hobbs, and U. Morgan-Ryan, "Morphology is not a reliable tool for delineating species within Cryptosporidium.," *J. Parasitol.*, vol. 89, no. 2, pp. 399–402, Apr. 2003, doi: 10.1645/0022-3395(2003)089[0399:MINART]2.0.CO;2.

[42] S. A. Henriksen and J. F. Pohlenz, "Staining of cryptosporidia by a modified Ziehl-Neelsen technique.," *Acta Vet. Scand.*, vol. 22, no. 3–4, pp. 594–596, 1981, doi: 10.1186/BF03548684.

[43] H. V Smith, B. M. Campbell, C. A. Paton, and R. A. B. Nichols, "Significance of enhanced morphological detection of Cryptosporidium sp. oocysts in water concentrates determined by using 4',6'-diamidino-2-phenylindole and immunofluorescence microscopy.," *Appl. Environ. Microbiol.*, vol. 68, no. 10, pp. 5198–5201, Oct. 2002, doi: 10.1128/AEM.68.10.5198-5201.2002.

[44] L. S. Garcia and R. Y. Shimizu, "Evaluation of nine immunoassay kits (enzyme immunoassay and direct fluorescence) for detection of Giardia lamblia and Cryptosporidium parvum in human fecal specimens.," *J. Clin. Microbiol.*, vol. 35, no. 6, pp. 1526–1529, Jun. 1997, doi: 10.1128/jcm.35.6.1526-1529.1997.

[45] S. P. Johnston, M. M. Ballard, M. J. Beach, L. Causer, and P. P. Wilkins, "Evaluation of three commercial assays for detection of Giardia and Cryptosporidium organisms in fecal specimens.," *J. Clin. Microbiol.*, vol. 41, no. 2, pp. 623–626, Feb. 2003, doi: 10.1128/JCM.41.2.623-626.2003.

[46] C. Weir, G. Vesey, M. Slade, B. Ferrari, D. A. Veal, and K. Williams, "An immunoglobulin G1 monoclonal antibody highly specific to the wall of Cryptosporidium oocysts," *Clin. Diagn. Lab. Immunol.*, vol. 7, no. 5, pp. 745–750, 2000, doi: 10.1128/CDLI.7.5.745-750.2000.

[47] B. C. Ferrari, G. Vesey, C. Weir, K. L. Williams, and D. A. Veal, "Comparison of Cryptosporidium-specific and Giardia-specific monoclonal antibodies for monitoring water samples," *Water Res.*, vol. 33, no. 7, pp. 1611–1617, 1999, doi: 10.1016/S0043-1354(98)00398-4.

[48] E. M. Hassan, B. Örmeci, M. C. DeRosa, B. R. Dixon, S. A. Sattar, and A. Iqbal, "A review of Cryptosporidium spp. And their detection in water," *Water Sci. Technol.*, vol. 83, no. 1, pp. 1–25, 2021, doi: 10.2166/wst.2020.515.

[49] C. Thiruppathiraja, V. Saroja, S. Kamatchiammal, P. Adaikkappan, and M. Alagar, "Development of electrochemical based sandwich enzyme linked immunosensor for Cryptosporidium parvum detection in drinking water," *J. Environ. Monit.*, vol. 13, no. 10, pp. 2782–2787, 2011, doi: 10.1039/c1em10372e.

[50] A. Iqbal, M. Labib, D. Muharemagic, S. Sattar, B. R. Dixon, and M. V. Berezovski, "Detection of Cryptosporidium parvum oocysts on fresh produce using DNA aptamers," *PLoS One*, vol. 10, no. 9, pp. 1–13, 2015, doi: 10.1371/journal.pone.0137455.

[51] A. Iqbal, J. Liu, B. Dixon, B. Zargar, and S. A. Sattar, "Development and application of DNA-aptamer-coupled magnetic beads and aptasensors for the detection of Cryptosporidium parvum oocysts in drinking and recreational water resources.," *Can. J. Microbiol.*, vol. 65, no. 11, pp. 851–857, Nov. 2019, doi: 10.1139/cjm-2019-0153.

[52] H. Bridle *et al.*, "Detection of Cryptosporidium in miniaturised fluidic devices," *Water Res.*, vol. 46, no. 6, pp. 1641–1661, 2012, doi: 10.1016/j.watres.2012.01.010.

[53] S. R. Nugen, P. J. Asiello, J. T. Connelly, and A. J. Baeumner, "PMMA biosensor for nucleic acids with integrated mixer and electrochemical detection.," *Biosens. Bioelectron.*, vol. 24, no. 8, pp. 2428–2433, Apr. 2009, doi: 10.1016/j.bios.2008.12.025.

[54] A. E. Grow, L. L. Wood, J. L. Claycomb, and P. A. Thompson, "New biochip technology for label-free detection of pathogens and their toxins.," *J. Microbiol. Methods*, vol. 53, no. 2, pp. 221–233, May 2003, doi: 10.1016/s0167-7012(03)00026-5.

[55] K. Rule and P. J. Vikesland, "Surface-enhanced resonance raman

spectroscopy for the rapid detection of cryptosporidium parvum and giardia lamblia," *Environ. Sci. Technol.*, vol. 43, no. 4, pp. 1147–1152, 2009, doi: 10.1021/es801531t.

[56] G. Luka, E. Samiei, N. Tasnim, A. Dalili, H. Najjaran, and M. Hoorfar, "Comprehensive review of conventional and state-of-the-art detection methods of Cryptosporidium," *J. Hazard. Mater.*, vol. 421, no. July 2021, 2022, doi: 10.1016/j.jhazmat.2021.126714.

[57] C. D. Kang, S. W. Lee, T. H. Park, and S. J. Sim, "Performance enhancement of real-time detection of protozoan parasite, Cryptosporidium oocyst by a modified surface plasmon resonance (SPR) biosensor," *Enzyme Microb. Technol.*, vol. 39, no. 3, pp. 387–390, 2006, doi: 10.1016/j.enzmictec.2005.11.039.

[58] C. D. Kang, C. Cao, J. Lee, I. S. Choi, B. W. Kim, and S. J. Sim, "Surface plasmon resonance-based inhibition assay for real-time detection of Cryptosporidium parvum oocyst," *Water Res.*, vol. 42, no. 6–7, pp. 1693–1699, 2008, doi: 10.1016/j.watres.2007.10.023.

[59] S. Jain, T. G. Costa Melo, S. S. Dolabella, and J. Liu, "Current and emerging tools for detecting protozoan cysts and oocysts in water," *TrAC - Trends Anal. Chem.*, vol. 121, p. 115695, 2019, doi: 10.1016/j.trac.2019.115695.

[60] G. A. Campbell and R. Mutharasan, "Near real-time detection of Cryptosporidium parvum oocyst by IgM-functionalized piezoelectric-excited millimeter-sized cantilever biosensor," *Biosens. Bioelectron.*, vol. 23, no. 7, pp. 1039–1045, 2008, doi: 10.1016/j.bios.2007.10.017.

[61] S. Xu and R. Mutharasan, "Detection of Cryptosporidium parvum in buffer and in complex matrix using PEMC sensors at 5oocystsmL-1," *Anal. Chim. Acta*, vol. 669, no. 1–2, pp. 81–86, 2010, doi: 10.1016/j.aca.2010.04.056.

[62] M. B. Esch, A. J. Baeumner, and R. A. Durst, "Detection of Cryptosporidium parvum using oligonucleotide-tagged liposomes in a competitive assay format.," *Anal. Chem.*, vol. 73, no. 13, pp. 3162–3167, Jul. 2001, doi: 10.1021/ac010012i.

[63] M. B. Esch, L. E. Locascio, M. J. Tarlov, and R. A. Durst, "Detection of viable Cryptosporidium parvum using DNA-modified liposomes in a microfluidic chip.," *Anal. Chem.*, vol. 73, no. 13, pp. 2952–2958, Jul. 2001, doi: 10.1021/ac001508n.

[64] N. Kumar and S. Kumbhat, *Essentials in nanoscience and nanotechnology*. New Jersey: John Wiley & Sons, 2016.

[65] B. D. Malhotra and M. A. Ali, "Nanomaterials in Biosensors: Fundamentals and Applications.," *Nanomaterials for Biosensors*. pp. 1–74, 2018, doi: 10.1016/B978-0-323-44923-6.00001-7.

[66] K. E. Sapsford *et al.*, "Functionalizing nanoparticles with biological molecules: Developing chemistries that facilitate nanotechnology," *Chem.*

Rev., vol. 113, no. 3, pp. 1904–2074, 2013, doi: 10.1021/cr300143v.

[67] X. Hu, Y. Zhang, T. Ding, J. Liu, and H. Zhao, "Multifunctional Gold Nanoparticles: A Novel Nanomaterial for Various Medical Applications and Biological Activities," *Front. Bioeng. Biotechnol.*, vol. 8, no. August, pp. 1–17, 2020, doi: 10.3389/fbioe.2020.00990.

[68] Y. Li, H. J. Schluesener, and S. Xu, "Gold nanoparticle-based biosensors," *Gold Bull.*, vol. 43, no. 1, pp. 29–41, 2010.

[69] N. H. Kim, T. J. Baek, H. G. Park, and G. H. Seong, "Highly sensitive biomolecule detection on a quartz crystal microbalance using gold nanoparticles as signal amplification probes.," *Anal. Sci. Int. J. Japan Soc. Anal. Chem.*, vol. 23, no. 2, pp. 177–181, Feb. 2007, doi: 10.2116/analsci.23.177.

[70] P. Jiang, Y. Wang, L. Zhao, C. Ji, D. Chen, and L. Nie, "Applications of gold nanoparticles in non-optical biosensors," *Nanomaterials*, vol. 8, no. 12, pp. 1–23, 2018, doi: 10.3390/nano8120977.

[71] M. Ozsoz *et al.*, "Electrochemical genosensor based on colloidal gold nanoparticles for the detection of Factor V Leiden mutation using disposable pencil graphite electrodes.," *Anal. Chem.*, vol. 75, no. 9, pp. 2181–2187, May 2003, doi: 10.1021/ac026212r.

[72] S. Afonso, B. Pe, M. M. Costa, A. Merkoc, and A. X. Roig-sague, "Biosensors and Bioelectronics Electrochemical detection of Salmonella using gold nanoparticles," *Biosens. Bioelectron.*, vol. 40, pp. 121–126, 2013, doi: 10.1016/j.bios.2012.06.054.

[73] M. Rochelet-dequaire, "Subfemtomolar electrochemical detection of target DNA by catalytic enlargement of the hybridized gold nanoparticle labels," no. Iii, pp. 923–929, 2006, doi: 10.1039/b603963d.

[74] S. J. Amina and B. Guo, "A review on the synthesis and functionalization of gold nanoparticles as a drug delivery vehicle," *Int. J. Nanomedicine*, vol. 15, pp. 9823–9857, 2020, doi: 10.2147/IJN.S279094.

[75] J. Dong, P. L. Carpinone, G. Pyrgiotakis, P. Demokritou, M. Brij, and S. Systems, "Synthesis of Precision Gold Nanoparticles Using Turkevich Method," *Kona*, vol. 37, pp. 224–232, 2020, doi: 10.14356/kona.2020011.Synthesis.

[76] P. Zhao, N. Li, and D. Astruc, "State of the art in gold nanoparticle synthesis," *Coord. Chem. Rev.*, vol. 257, no. 3–4, pp. 638–665, 2013, doi: 10.1016/j.ccr.2012.09.002.

[77] N. R. Jana, L. Gearheart, and C. J. Murphy, "Seed-mediated growth approach for shape-controlled synthesis of spheroidal and rod-like gold nanoparticles using a surfactant template," *Adv. Mater.*, vol. 13, no. 18, pp. 1389–1393, 2001.

[78] M. H. Jazayeri, H. Amani, A. A. Pourfatollah, H. Pazoki-Toroudi, and B.

Sedighimoghaddam, “Various methods of gold nanoparticles (GNPs) conjugation to antibodies,” *Sens. Bio-Sensing Res.*, vol. 9, pp. 17–22, 2016, doi: 10.1016/j.sbsr.2016.04.002.

[79] R. A. Sperling and W. J. Parak, “Surface modification, functionalization and bioconjugation of colloidal Inorganic nanoparticles,” *Philos. Trans. R. Soc. A Math. Phys. Eng. Sci.*, vol. 368, no. 1915, pp. 1333–1383, 2010, doi: 10.1098/rsta.2009.0273.

[80] K. C. Grabar, M. B. Hommer, M. J. Natan, and R. G. Freeman, “Preparation and Characterization of Au Colloid Monolayers,” *Anal. Chem.*, vol. 67, no. 4, pp. 735–743, 1995, doi: 10.1021/ac00100a008.

[81] V. Amendola and M. Meneghetti, “Size evaluation of gold nanoparticles by UV-vis spectroscopy,” *J. Phys. Chem. C*, vol. 113, no. 11, pp. 4277–4285, 2009, doi: 10.1021/jp8082425.

[82] N. D. Samsuri *et al.*, “Synthesis methods of gold nanoparticles for Localized Surface Plasmon Resonance (LSPR) sensor applications,” in *EPJ Web of Conferences*, 2017, vol. 01002, pp. 1–5, doi: 10.1051/epjconf/201716201002.

[83] S. K. Brar and M. Verma, “Measurement of nanoparticles by light-scattering techniques,” *TrAC - Trends Anal. Chem.*, vol. 30, no. 1, pp. 4–17, 2011, doi: 10.1016/j.trac.2010.08.008.

[84] R. Pecora, “Dynamic light scattering measurement of nanometer particles in liquids,” *J. nanoparticle Res.*, vol. 2, no. 2, pp. 123–131, 2000.

[85] P. M. Carvalho, M. R. Felício, N. C. Santos, S. Gonçalves, and M. M. Domingues, “Application of light scattering techniques to nanoparticle characterization and development,” *Front. Chem.*, vol. 6, no. June, pp. 1–17, 2018, doi: 10.3389/fchem.2018.00237.

[86] Q. Wei, F. Huang, and Y. Cai, “2 - Textile surface characterization methods,” in *Surface Modification of Textiles*, Q. Wei, Ed. Woodhead Publishing, 2009, pp. 26–57.

[87] S. Sinha Ray, “4 - Techniques for characterizing the structure and properties of polymer nanocomposites,” in *Environmentally Friendly Polymer Nanocomposites*, S. Sinha Ray, Ed. Woodhead Publishing, 2013, pp. 74–88.

[88] N. Elgrishi, K. J. Rountree, B. D. McCarthy, E. S. Rountree, T. T. Eisenhart, and J. L. Dempsey, “A Practical Beginner’s Guide to Cyclic Voltammetry,” *J. Chem. Educ.*, vol. 95, no. 2, pp. 197–206, 2018, doi: 10.1021/acs.jchemed.7b00361.

[89] H. Robson, M. Reinhardt, and C. Bracher, “Cyclic Voltammetry Basic Principles, Theory and Setup.” https://www.ossila.com/pages/cyclic-voltammetry (accessed Aug. 05, 2022).

[90] P. T. Kissinger and W. R. Heineman, “Cyclic voltammetry,” *J. Chem.*

Educ., vol. 60, no. 9, p. 702, Sep. 1983, doi: 10.1021/ed060p702.

[91] Y. Q. He, S. P. Liu, L. Kong, and Z. F. Liu, "A study on the sizes and concentrations of gold nanoparticles by spectra of absorption , resonance Rayleigh scattering and resonance non-linear scattering," *Spectrochim. Acta*, vol. 61, no. 13–14, pp. 2861–2866, 2005, doi: 10.1016/j.saa.2004.10.035.

[92] M. A. Dheyab *et al.*, "Monodisperse Gold Nanoparticles: A Review on Synthesis and Their Application in Modern Medicine," *Int. J. Mol. Sci.*, vol. 23, no. 13, 2022, doi: 10.3390/ijms23137400.

[93] X. Ji, X. Song, J. Li, Y. Bai, and W. Yang, "Size Control of Gold Nanocrystals in Citrate Reduction: The Third Role of Citrate Xiaohui," *J. Am. Chem. Soc.*, vol. 129, no. 8, pp. 13939–13948, 2007.

[94] H. Tyagi, A. Kushwaha, A. Kumar, and M. Aslam, "A Facile pH Controlled Citrate-Based Reduction Method for Gold Nanoparticle Synthesis at Room Temperature," *Nanoscale Res. Lett.*, vol. 11, no. 1, 2016, doi: 10.1186/s11671-016-1576-5.

[95] M. Danaei *et al.*, "Impact of particle size and polydispersity index on the clinical applications of lipidic nanocarrier systems," *Pharmaceutics*, vol. 10, no. 2, pp. 1–17, 2018, doi: 10.3390/pharmaceutics10020057.

[96] H. S. Magar, R. Y. A. Hassan, and A. Mulchandani, "Electrochemical impedance spectroscopy (Eis): Principles, construction, and biosensing applications," *Sensors*, vol. 21, no. 19, 2021, doi: 10.3390/s21196578.

[97] R. A. Olowu, O. Arotiba, S. N. Mailu, T. T. Waryo, P. Baker, and E. Iwuoha, "Electrochemical aptasensor for endocrine disrupting 17β-estradiol based on a Poly(3,4-ethylenedioxylthiopene)-gold nanocomposite platform," *Sensors (Switzerland)*, vol. 10, no. 11, pp. 9872–9890, 2010, doi: 10.3390/s101109872.

[98] G. Fomo, T. T. Waryo, C. E. Sunday, A. A. Baleg, P. G. Baker, and E. I. Iwuoha, "Aptameric Recognition-Modulated Electroactivity of Poly(4-Styrenesolfonic Acid)-Doped Polyaniline Films for Single-Shot Detection of Tetrodotoxin," *Sensors*, vol. 15, pp. 22547–22560, 2015, doi: 10.3390/s150922547.